

**MAPPING THE SUBSURFACE STRUCTURE OF THE BOSUMTWE
IMPACT CRATER USING GROUND PENETRATING RADAR (GPR)**

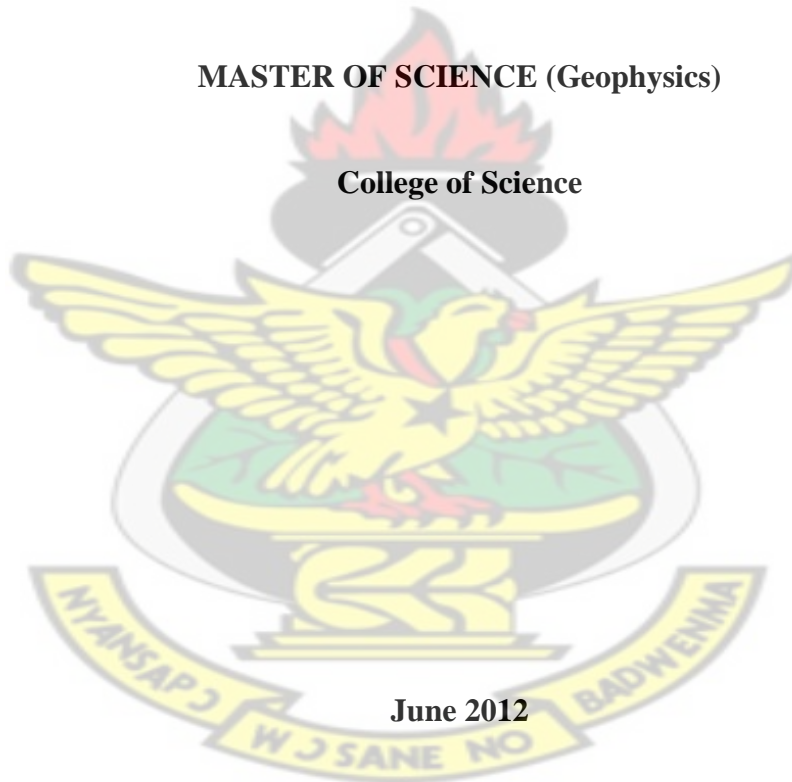
By

Cyril Dzedzorm Boateng (BSc Chemical Engineering)

**A Thesis submitted to the Department of Physics, Kwame Nkrumah University
of Science and Technology in partial fulfilment of the requirements for the
degree**

MASTER OF SCIENCE (Geophysics)

College of Science



June 2012

Supervisor (Prof S. K. Danuor)

ABSTRACT

The Bosumtwe crater in Ghana, is a unique structure and ecosystem on earth. It is one of the 19 impact craters known in Africa. The crater is located 30 km southwest of the city of Kumasi in the Ashanti Region of Ghana. The Bosumtwe crater is 1.07 million years old and is almost completely filled with a lake which is 8.5 km in diameter. This has made the Bosumtwe crater a location of prime importance to the scientific community. Other reasons for interest in the Bosumtwe crater are; the visits of over a 100,000 tourists to the area each year leading to the development of numerous tourists resorts, the presence of over 24 communities within the crater whose sustenance depends on the sustainability of the crater, and the presence of known gold deposits. The challenge is to use modern scientific methods to solve and prevent future problems such as landslides, collapse of buildings and contamination of the lake that may arise. One of the effective set of tools for studying the subsurface is near surface geophysics. Ground penetrating radar (GPR) was used in this case because of its higher resolution and the ability to show more detail. In recent years, this method has evolved into the fastest growing geophysical method worldwide. This study had the objective of delineating subsurface structures such as the depth to bedrock; the water table; the fracture pattern, distribution and orientation within the crater; and also find out if fractures serve as potential fluid migration paths for contaminants to enter the lake. Radar methods use the reflections of short bursts of electromagnetic energy (chirps) spanning a range of frequencies from about 50% below to 50% above some specified central frequency. The Mala GPR system using 25 MHz and 50 MHz RTA was used for conducting the geophysical survey. 20 GPR profiles were taken across the northern section of the inner morphological crater. The digital data gathered was processed using Sandmeier's Reflex-Win software and

three migration algorithms were used namely; diffraction stack, f-k (Stolt) and Kirchoff. Various subsurface features were delineated. These include unconsolidated breccia layer, shattered bedrock, fractures, duplex or lens shaped bodies, and a coherent water table. The depth to bedrock varies between 5 m to 20 m. The depth to water table also varies between 5 m to 20 m. Within the inner morphological crater, multiple fractures with different orientations occur. The water table within the inner morphological crater is at a similar elevation as the surface of the lake. Movement of groundwater into the lake is negligible. The water table within the crater is largely influenced by the water level within the lake. There is a high possibility of contamination of the lake from agrochemicals used for cocoa farming within the crater migrating through the fractures into the lake. The resort towns of Abonu and Obo have a high occurrence of fractures and this information is relevant for engineering sustainable resorts in these towns. The diffraction stack algorithm successfully migrated hyperbolas and the subsurface features to their correct depths.

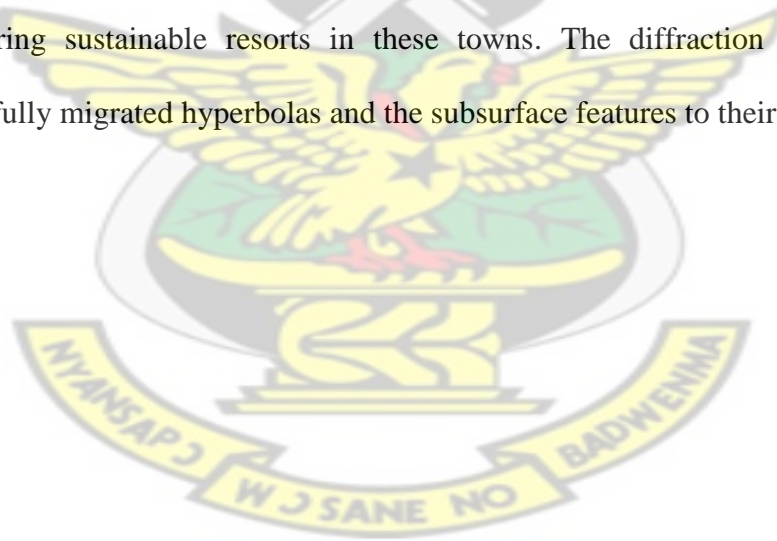
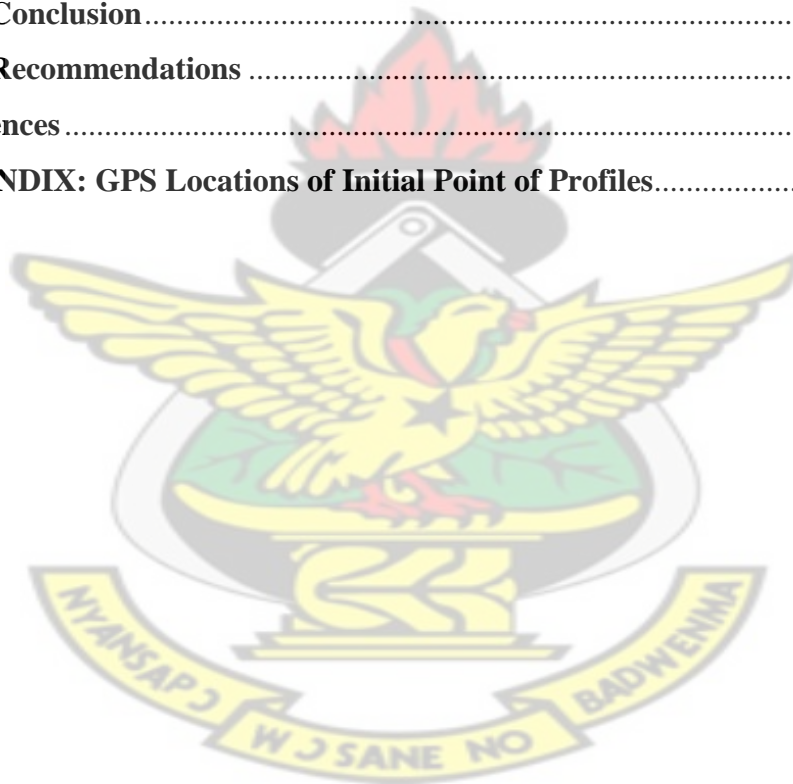


Table of Contents

Title Page.....	i
Declaration.....	ii
Abstract.....	iii
Table of Contents.....	v
Figures.....	viii
Tables.....	xi
Acknowledgements.....	xii
Dedication.....	xiii
CHAPTER ONE	1
1.0 Introduction.....	1
1.1 The Scientific Challenge	1
1.2 The Problem.....	3
1.3 Objectives.....	4
1.4 Study area	4
1.4.1 Location and Origins.....	5
1.4.2 Climate and Physical Characteristics	7
1.5 Layout of Thesis	7
CHAPTER TWO	9
2.0 Literature Review.....	9
2.1 Ground Penetrating Radar	9
2.1.1 Basics and History	9
2.1.2 Electromagnetic Theory.....	11
2.1.3 GPR Theory	12
2.1.4 Energy Losses.....	13
2.1.5 Resolution	16
2.1.6 Dielectric Properties of Geological Materials	17
2.1.7 Mode of Data Acquisition	17
2.1.8 Interference in GPR Surveys.....	18
2.1.9 Data Processing.....	18
2.2 Impact Craters.....	19

2.2.1 Significance of Impact Craters	19
2.2.2 The Impact Cratering Process.....	20
2.2.3 GPR Investigations in Crater Terrains	21
2.3 Geological Overview of the Bosumtwe Impact Crater	22
2.3.1 The Birimian Supergroup.....	22
2.3.2 The Tarkwaian Supergroup	23
2.3.3 Dikes and Intrusives	23
2.3.4 Breccia	23
CHAPTER THREE	26
3.0 Materials and Methods.....	26
3.1 GPR Equipment	26
3.2 Data Acquisition	27
3.3 Data Processing	29
CHAPTER FOUR.....	32
4.0 Results and Interpretation	32
4.1 Migration Algorithms	32
4.2 Profile Sections	38
4.2.1 Profile 1.....	38
4.2.2 Profile 2.....	38
4.2.3 Profile 3.....	39
4.2.4 Profile 4.....	40
4.2.5 Profile 5.....	41
4.2.6 Profile 6.....	42
4.2.7 Profile 7.....	43
4.2.8 Profile 8.....	43
4.2.9 Profile 9.....	44
4.2.10 Profile 10.....	45
4.2.11 Profile 11.....	46
4.2.12 Profile 12.....	47
4.2.13 Profile 15.....	48
4.2.14 Profile 16.....	49
4.2.15 Profile 17.....	50
4.2.16 Profile 18.....	51

4.2.17 Profile 19.....	51
4.2.18 Profile 20.....	52
4.2.19 Profile 21.....	53
4.2.20 Profile 22.....	53
4.3 Interpretations of Radargrams	54
4.4 Stratigraphic Horizons	55
4.4.1 Bedrock Layer.....	56
4.5 Depth to Water table.....	57
4.6 Fracture Distribution.....	59
CHAPTER FIVE	61
5.0 Conclusion and Recommendations	61
5.1 Conclusion.....	61
5.2 Recommendations	62
References	64
APPENDIX: GPS Locations of Initial Point of Profiles.....	69



LIST OF FIGURES

Figure 1.1: Schematic overview of Bosumtwe crater location and relation to the Ivory Coast tektite strewn field (C. Koeberl, W. U. Reimold, et al. 1998).....	5
Figure 1.2: Section of impact crater covered by survey (not to scale).....	6
Figure 1.3: Panoramic views of the Bosumtwe impact crater and lake (Koeberl and Reimold 2005).....	6
Figure 2.1: Simplified diagram of the constituents of a radar system (Reynolds, 1997).....	10
Figure 2.2: Processes that lead to reduction in signal strength (Reynolds, 1997).....	14
Figure 2.3: Simplified sketches of the excavation and modification stages during the formation of a complex impact crater (Melosh, 1989).....	21
Figure 2.4: Extract of a radar sounding (Heggy and Paillou, 2006).....	22
Figure 2.5: Zonation of northwestern crater rim: Zone 1; dominantly ejecta breccias cover and local mass wasting. Zone 2; inward dipping thrust planes, conjugate radial fractures, isoclinal folding, and overturned stratigraphy. Zone 3; megabreccia with upward decreasing block sizes. Zone 4; dominant thrust faulting of multiple orientations, resulting in duplex and lens shaped bodies of pre-impact strata (Reimold, Brandt & Koeberl, 1998).....	24
Figure 2.5: Geological map of the Bosumtwe impact crater (compiled by Koeberl and Reimold, 2005).....	25
Figure 3.1: The Mala GPR system used for the survey.....	26

Figure 3.2: Locations of profiles.....	27
Figure 3.3: Images from the data acquisition stage.....	31
Figure 4.1: Profile 1 obtained with the 25 MHz RTA and migrated with (A) diffraction stack algorithm (B) Kirchoff algorithm (C) f-k algorithm.....	32
Figure 4.2: Profile 2 obtained with the 25 MHz RTA and migrated with (A) diffraction stack algorithm (B) Kirchoff algorithm (C) f-k algorithm.....	33
Figure 4.3: Profile 18 obtained with the 25 MHz RTA and migrated with (A) diffraction stack algorithm (B) Kirchoff algorithm (C) f-k algorithm.....	34
Figure 4.4: Profile 21 obtained with the 25 MHz RTA and migrated with (A) diffraction stack algorithm (B) Kirchoff algorithm (C) f-k algorithm.....	35
Figure 4.5: Comparison of (A) 50 MHz and (B) 25 MHz sections of Profile 9.....	36
Figure 4.6: Comparison of (A) 50 MHz and (B) 25 MHz sections of Profile 16.....	37
Figure 4.7: Profile 1 showing marked anomalies.....	39
Figure 4.8: Profile 2 showing marked anomalies.....	39
Figure 4.9: Profile 3 showing marked anomalies.....	40
Figure 4.10: Profile 4 showing marked anomalies.....	41
Figure 4.11: Profile 5 showing marked anomalies.....	41
Figure 4.12: Profile 6 showing marked anomalies.....	42
Figure 4.13: Profile 7 showing marked anomalies.....	43
Figure 4.14: Profile 8 showing marked anomalies.....	44
Figure 4.15: Profile 9 showing marked anomalies.....	45

Figure 4.16: Profile 10 showing marked anomalies.....	46
Figure 4.17: Profile 11 obtained showing marked anomalies.....	47
Figure 4.18: Profile 12 showing marked anomalies.....	48
Figure 4.19: Profile 15 showing marked anomalies.....	49
Figure 4.20: Profile 16 showing marked anomalies.....	49
Figure 4.21: Profile 17 showing marked anomalies.....	51
Figure 4.22: Profile 18 showing marked anomalies.....	51
Figure 4.23: Profile 19 showing marked anomalies.....	52
Figure 4.24: Profile 20 showing marked anomalies.....	52
Figure 4.25: Profile 21 showing marked anomalies.....	53
Figure 4.26: Profile 22 showing marked anomalies.....	54
Figure 4.27: Depth to bedrock variation within Bosumtwe Crater.....	56
Figure 4.28: A classed post map show water table variation within the Northern section of the Bosumtwe impact crater.....	57
Figure 4.29: A post map showing fracture distribution within the northern sector of Bosumtwe crater.....	59

LIST OF TABLES

Table 3.1: Profile names, lengths and directions.....	28
Table 3.2: Acquisition parameters of GPR survey.....	30
Table 4.1: Water table elevation and lake level elevation.....	58

KNUST



ACKNOWLEDGEMENTS

Firstly, thanks go to the Almighty God who has kept me through the duration of the project. Secondly, my supervisors Professor S. K. Danuor and Mr Van-Dycke Asare have been fantastic in guiding me to this point of my studies and I greatly appreciate their support. Thirdly and finally, I am grateful to my family.

KNUST



DEDICATION

This work is dedicated to my Dad, Victor Kofi Aburu, my mentor, my inspiration who passed on during my MSC studies.

KNUST



CHAPTER ONE

INTRODUCTION

1.0 Introduction

1.1 The Scientific Challenge

Planet Earth has a lot of unique ecosystems and natural environments. A better understanding of modes of formation of features on earth and the changes that they have undergone over time will help man better manage the Earth. This is especially in the context of contemporary concerns over sustainable methods of managing the Earth and global environmental concerns. The UN Millenium Development Goal 7 for example covers ensuring environmental sustainability (United Nations, 2010). The effects of man's activities on the environment of Earth and geological processes which have taken place over millions of years have changed the face of the Earth over time. The challenge is to use modern scientific methods to solve and prevent future problems that may arise. With the advancement of science in modern times a better understanding of the Earth can be gotten through the use of the scientific methods in investigating current situations and causes of problems.

The Bosumtwe crater in Ghana, is a unique structure and ecosystem on Earth. It is one of the 19 impact craters known in Africa (Koeberl and Reimold, 2005) and has the distinction of being associated with one of the four tektite strewn fields in the world and therefore is of world class scientific importance (Koeberl, 1994a; Koeberl, et al. 1997a). This has made Lake Bosumtwe a location of prime importance to the scientific community. In addition, it is a key tourist location in Ghana with over a 100,000 tourists visiting the lake and its surroundings each year (Bosumtwe District Assembly, 2006). There are also several communities located around the lake with their sustenance based on fishing in the lake and on farming in the crater structure.

Finally, there has been a strong geological interest in the crater area due to the presence of known gold deposits (Koeberl & Reimold, 2005).

Due to the mode of formation of the crater, environmental and engineering questions have arisen which require a solid scientific basis for investigations and for solutions to be proffered. Relevant scientific information is required to inform and create awareness about the environmental problems at the Bosumtwé crater; problems which are associated with crater formation and which need to be addressed for sustainable management of the lake in the crater and other resources in the crater structure.

This study intends to focus on delineating the subsurface structures in the inner morphological crater. An effective set of tools for studying the subsurface is near surface geophysics. It can be an effective scientific method for gaining additional information on the subsurface structure of the crater. According to Steeples (2001), near surface measurements and geologic interpretations generally are applied for the following reasons; to mitigate existing engineering and environmental problems and as input to design parameters used to prevent future engineering and environmental problems. This statement satisfies the goals of the survey. Geophysics was traditionally a tool for the exploration of natural resources such as hydrocarbons and minerals. The use of geophysics in hydrocarbon exploration has had to deal with depths of up to hundreds of kilometers. Over the years however, geophysics has developed to the stage where it is applied to a wide spectrum of problems which cover a depth of only zero to a few hundred meters. Near surface geophysics is defined as investigating the uppermost fifty to hundred meters (50 m-100 m) of the earth's subsurface and the methods used include gravity, magnetic, electrical resistivity, self potential (SP), electromagnetics, ground penetrating radar (GPR),

seismic reflection, seismic refraction and other methods (SEG, 2012).

When the objective of the study is achieved the stock of information available on the impact crater will increase and aid in the effective management of such a unique structure.

1.2 The Problem

The Bosumtwe crater and the lake area form a serene environment with immense tourism and scientific potential. Hundreds of thousands of tourists throng the lakeside and its surrounding communities each year. Scientific research has also been conducted in the crater and on the lake. The lake is of immense significance to paleoclimatologists as a location which can be used in understanding climatic records over thousands of years. Over 24 communities also depend on the lake and its environment. Due to these reasons the crater, lake and surroundings need to be preserved and effectively managed.

The Lake Bosumtwe crater was formed by meteorite impact. Associated with this mode of formation is considerable tectonic disturbance of the subsurface structure. As a result, subsurface rocks are highly shattered and fractured, with faults and weak zones dominating the tectonic setting (Danour, 2012). Attendant problems which have arisen due to the nature of the subsurface are: landslides which can cause erosion; fracturing and shattering of the rocks, which cause buildings to collapse in crater area; contaminants from agrochemicals, mining activities and communities migrating through the fractures and fissures into the lake. The impact of these problems is myriad. One of these is the potential of fast siltation of the lake with disastrous consequences for the aquatic life and the fragile ecosystem (Danour, 2012). It will also mean a destruction of the livelihood base for the communities around the lake who depend on the lake as a source of income through fishing. The

tourism industry which depends on the existence of the lake will be adversely affected. Another possible negative effect of the shattered subsurface structure is the development of cracks or even total collapse of hotels, resorts and homes in the crater area due to the fragile nature of the subsurface. Fluid migration through existing fractures and fissures can also pollute the lake with agrochemicals from the many farms within the crater structure and from sewage from the many hotels and resorts being built around the lake.

To solve these problems the subsurface structure both within the morphological crater rim and the outer topographical rim needs to be mapped and characterized. This will inform the design and implementation of an effective management system of the lake and its surrounding resources. A non invasive, non destructive method for mapping the subsurface is the Ground Penetrating Radar (GPR). Ground penetrating radar (GPR) was used in this case because of its higher resolution and the ability to show more detail. In recent years this method has evolved into the fastest growing geophysical method worldwide.

1.3 Objectives

The primary objective of the project is to map the subsurface of the inner morphological crater using ground penetrating radar (GPR). From this primary objective the following secondary objectives can also be satisfied: determine the depth to bedrock; the water table; the fracture pattern, distribution and orientation within the crater; find out if fractures serve as potential fluid migration paths for contaminants to enter the lake; find out if groundwater is entering the lake by determining the water table outside the lake and determine the best processing algorithms for processing the GPR data.

1.4 Study area

1.4.1 Location and Origins

The Bosumtwe impact crater is located 30 km southeast of the city of Kumasi in the Ashanti Region of Ghana (shown in Figure 1.1). It is centred at 06°32'N and 01°25'W.

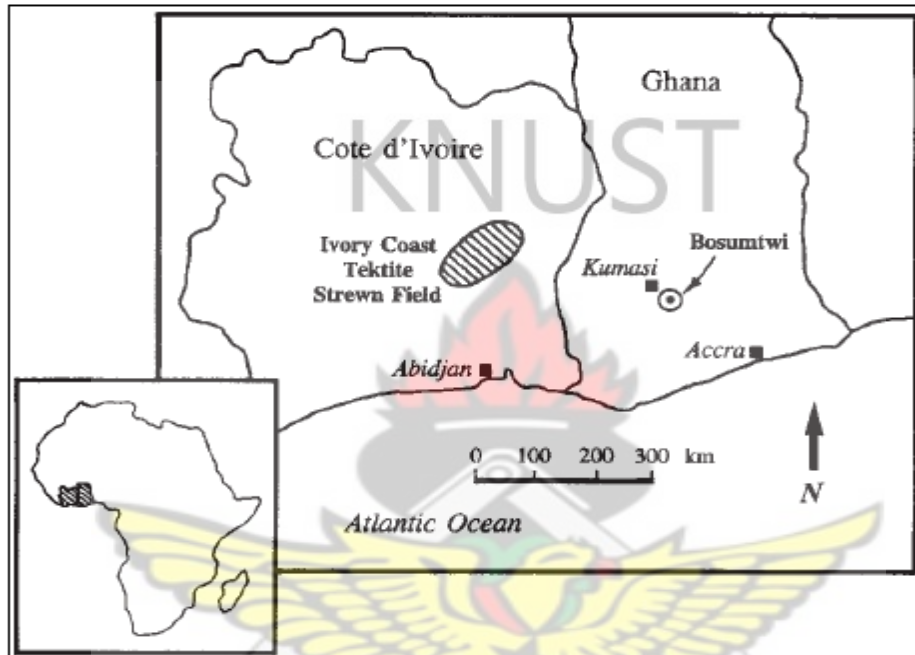


Fig. 1.1: Schematic overview of Bosumtwe crater location and relation to the Ivory Coast tektite strewn field (Koeberl, et al. 1998).

Bosumtwe is one of the 19 confirmed impact structures known in Africa and is the youngest well-preserved complex crater known on Earth (Koeberl and Reimold, 2005). The structure is 1.07 million years old and is almost completely filled with a lake which is 8.5 km in diameter (Koeberl and Reimold, 2005). Rim to rim diameter of the crater is 10.5 km. Bosumtwe is about 30 km from Kumasi. Figure 1.2 shows the section of the impact crater covered by the survey. Panoramic views of the crater structure and the lake are shown in figure 1.3.

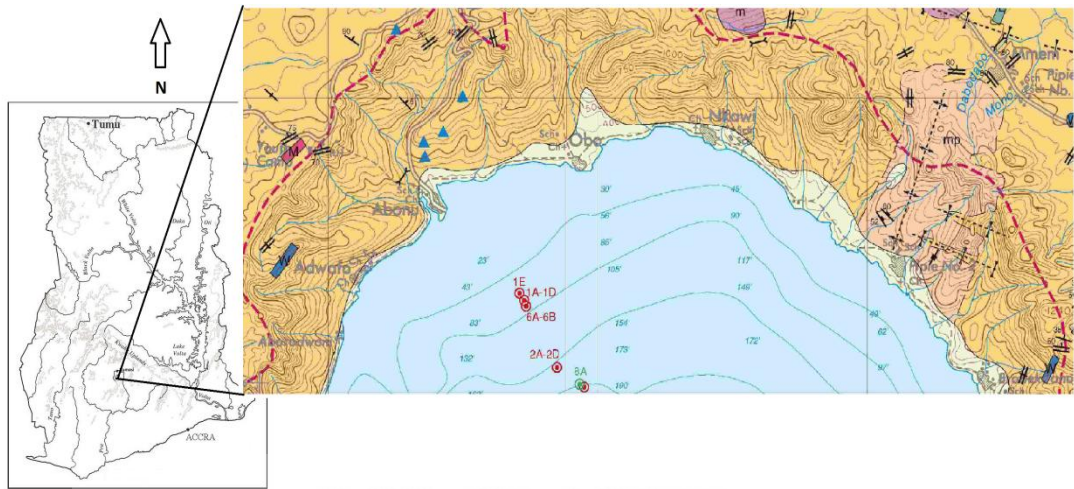


Fig. 1.2: Section of impact crater covered by survey (not to scale).



Fig. 1.3: Panoramic views of the Bosumtwi impact crater and lake (Koeberl and Reimold 2005).

1.4.2 Climate and Physical Characteristics

The crater is characterized by a depression which is filled by the lake and is surrounded by a crater rim at varied elevation. Information on the physical characteristics and climate was captured from the Bosomtwe District Assembly website (2006). Bosomtwe falls within the equatorial zone with a rainfall regime typical of the moist deciduous forest zone of Ghana.

Two rainy seasons occur in the area: a major season from March to July and a minor season from September to November. Temperature in the area is uniformly high with the mean temperature being 24°C. Relative humidity ranges between 42.5% and 95% in the year. The area around Bosomtwe is largely covered by dense tropical forest and woodland.

1.5 Layout of Thesis

The thesis begins with an introduction to the scientific challenge for managing the unique structures on Earth of which the Bosomtwe crater is an example. The problem as identified at the Bosomtwe crater is then elaborated upon and objectives of the study are stated. Finally the introduction ends with a look at the study area and the layout of the research work.

The second chapter lays the foundation for using the ground penetrating radar (GPR) as a tool for delineating subsurface features in the structure specifically the depth to bedrock; the water table; and the fracture pattern, distribution and orientation within the crater. This begins with the theoretical framework for the ground penetrating radar (GPR) method, then takes a look at the morphology of impact craters and the work done in mapping such structures and finally ends with an in-depth analysis of the geology of the Bosomtwe impact structure.

Ground penetrating radar (GPR) equipment used and the mode of deployment are

tackled in the third chapter. This chapter includes a description of the location of profiles and the methodology of the study. Additionally, the different processing algorithms used in filtering the data are then treated in this chapter.

Chapter 4 deals with the results obtained from the data acquired in the field and their interpretation. Conclusions and recommendations, and references are presented in Chapter 5 and 6 respectively.

KNUST



CHAPTER TWO

LITERATURE REVIEW

2.0 Literature Review

2.1 Ground Penetrating Radar

2.1.1 Basics and History

Ground penetrating radar (GPR) is a relatively new tool and uses electromagnetic fields to probe lossy dielectric materials to detect structures and changes in properties within the materials (Annan, 2002). Historically, the GPR method was developed from the use of radio echo-sounding to determine ice thickness and it was soon realized that some penetration was being achieved into the deeper, unfrozen, ground and that the depth of investigation although unlikely to ever amount to more than a few tens of meters could be increased by processing techniques virtually identical to those applied to seismic reflection data (Milsom, 2003). The history and developments in the GPR method have been treated in Annan's paper of 2002. The use of radar from the 1900's to the 1950's was mainly in communication applications. From 1950 to 1955 attempts were made to image the subsurface using GPR. From 1955 onwards signaled the use of radiowaves in echo-sounding. From 1965, other applications on favorable geologic materials were also researched into. It was also the start of research into the use of radiowaves for sounding the surface of the moon. From the 1970's onwards further research into the applications of radiowaves in other geologic materials was also done. Works such as that by Olhoeft (1975; 1987) led to a much better understanding of the electrical properties of naturally occurring geological materials and the relationship between electrical conductivity and dielectric polarization of these materials. From the 1980's onwards, GPR found a wider range of applications due to the wider availability of technology.

Work was done in potash mines by Annan and Davis (1988) and in coal mines by Coon, Fowler and Schafers (1981) showed the varied applications GPR could be put to.

Applications of GPR have also been adequately elaborated upon in detection of fractures by Thierbach (1974); and Nickel et al. (1983); civil engineering and geological investigations by Huggenberger, et al. (1994); Davis and Annan (1989); and Doolittle (1993); and in archeological investigations by Bevan (1991) and Bevan and Kenyon (1975). In recent times, work has been done in 3-D radar imaging by Grasmueck (1996), Grasmueck, et. al (2005), and McClymont, et al. (2006).

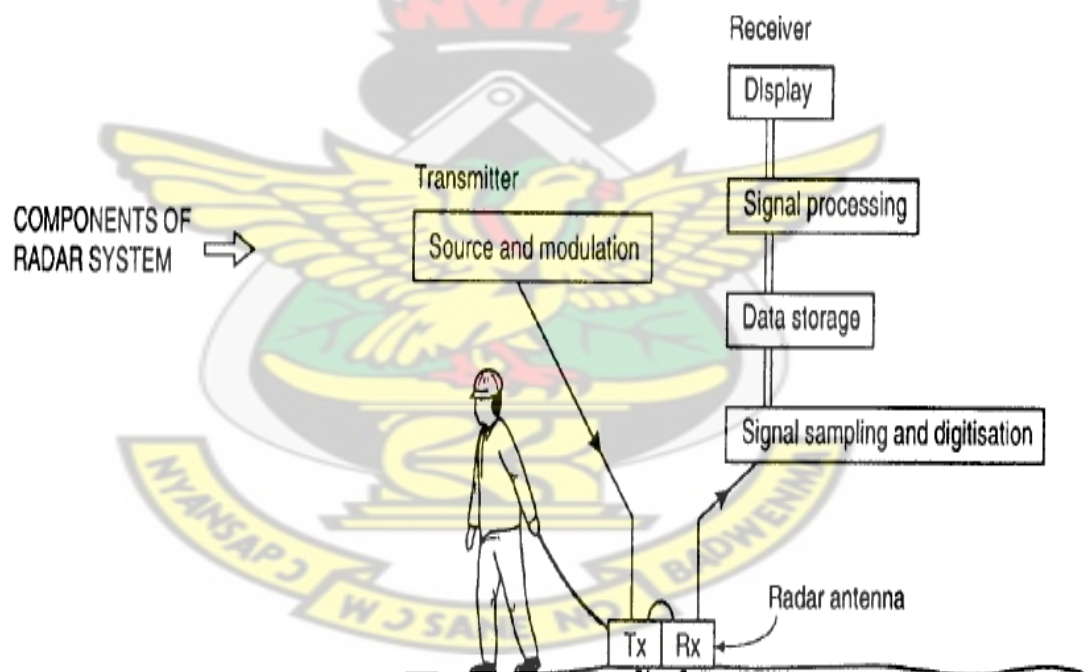


Fig. 2.1: Simplified diagram of the constituents of a radar system (Reynolds, 1997).

A radar system consists of a signal generator, transmitting and receiving antennas and a receiver with recording facilities. The basic constituents of a radar system are shown in Figure 2.1. The radar system causes the transmitter (Tx) to generate a wavetrain of radiowaves which propagates away in a broad beam. On encountering

obstacles, the wavetrain is refracted or reflected back to the receiving antenna (Rx). As the antennas are moved over the ground, the signals are displayed as a function of two-way travel time in the form of a radargram which is analogous to a seismic section.

2.1.2 Electromagnetic Theory

In GPR measurements, the radiation is electromagnetic and its propagation is described by Maxwell's equations. Maxwell's equations are given in equations 2.1, 2.2, 2.3 and 2.4,

$$\nabla \cdot D = \rho \dots \dots \dots (2.1) \text{ Gauss Law}$$

$$\nabla \cdot B = 0 \dots \dots \dots (2.2) \text{ Gauss law of magnetism}$$

$$\nabla \times E = -\frac{\partial B}{\partial t} \dots \dots \dots (2.3) \text{ Faraday's Law}$$

$$\nabla \times H = J + \frac{\partial D}{\partial t} \dots \dots \dots (2.4) \text{ Modified Ampere's Law}$$

where $E =$ Electric field intensity $\left[\frac{V}{m}\right]$, $H =$ Magnetic field intensity $\left[\frac{A}{m}\right]$

$J =$ Electric current density $\left[\frac{A}{m^2}\right]$, $D =$ Electric flux density $\left[\frac{C}{m^2}\right]$

$B =$ Magnetic flux density $[T]$, Electric charge density $\left[\frac{C}{m^3}\right]$

The constitutive relations introduce the material parameters, electric conductivity (σ), electric permittivity (ϵ) and magnetic permeability (μ).

$$J = \sigma E \dots \dots \dots (2.5)$$

$$D = \epsilon E \dots \dots \dots (2.6)$$

$$B = \mu H \dots \dots \dots (2.7)$$

From equation 2.1 to 2.7 one can derive the electromagnetic wave equation for the electric field:

$$\nabla^2 E - \mu\epsilon \frac{\partial^2 E}{\partial t^2} - \mu\sigma \frac{\partial E}{\partial t} = 0 \dots \dots \dots (2.8)$$

The wave equation for the magnetic flux density is exactly the same, by substituting **B** for **E** in equation 2.8.

$$\nabla^2 B = \mu\epsilon \frac{\partial^2 B}{\partial t^2} - \mu\sigma \frac{\partial B}{\partial t} = 0 \dots \dots \dots (2.9)$$

These two equations, 2.8 and 2.9 are not independent. If we find the electric field vector **E** from equation 2.8 we must return to Maxwell's equation to find the magnetic flux density **B** and vice versa. The resulting combination of the **E** and **B** fields is known as a transversal wave. E and B are perpendicular to each other as well as the direction of propagation.

2.1.3 GPR Theory

The following treatment of the theory of GPR and the principles of operation is largely drawn from Reynolds (1997) and Milsom (2003). Electromagnetic properties of materials are related to their composition and water content. Factors that determine the speed of radiowaves in any medium are therefore the speed of light in free space, the relative permittivity and the relative magnetic permeability. Relative permittivity used to be known as the relative dielectric constant.

$$v_m = \frac{c}{\left\{ \left(\frac{\epsilon_r \mu_r}{2} \right) [(1 + P^2) + 1] \right\}^{\frac{1}{2}}} \dots \dots \dots (2.10)$$

c is the speed of light in free space, ϵ_r is the relative permittivity, μ_r is the relative magnetic permeability, P is the loss factor.

$$P = \frac{\sigma}{\omega\epsilon} \dots \dots \dots (2.11)$$

σ is the conductivity,

$$\omega = 2\pi f$$

f is frequency, ϵ is the permittivity = $\epsilon_r \epsilon_0$

ϵ_0 is the permittivity of free space

The success of the ground radar method is dependent on the variability of the ground to allow the transmission of radiowaves. While some materials allow radiowaves to pass through them, others absorb or reflect these radiowaves. The contrast in relative permittivity between adjacent layers gives rise to the reflection of incident electromagnetic radiation. This is given by the reflection coefficient, R (equation 2.12 and 2.13).

$$R = \frac{V_1 - V_2}{V_1 + V_2} \dots \dots \dots (2.12)$$

R is the amplitude reflection coefficient,

where V_1 and V_2 are the radiowave velocities in layers 1 and 2 respectively

and $V_1 < V_2$

R can also be given as,

$$R = \frac{\sqrt{\epsilon_2} - \sqrt{\epsilon_1}}{\sqrt{\epsilon_2} + \sqrt{\epsilon_1}} \dots \dots \dots (2.13)$$

where ϵ_1 and ϵ_2 are the respective permittivities (ϵ_r) of layers 1 and 2,

ϵ_r increases with depth.

2.1.4 Energy Losses

There are processes that lead to the loss of signal strength during the use of the ground penetrating radar. Total path losses are attributable to antenna losses, transmission losses between the air and ground, losses caused by the geometrical spreading of the radar beam, attenuation within the ground as a function of the material properties and losses due to scattering of the radar signal from the target itself. Reflection/transmission losses about each interface cause energy losses anytime the radiowaves pass through a boundary. If there are objects with the same order of wavelength as the radar signal, they will cause scattering of energy in a

random manner. This is known as Mie scattering and is also another cause of loss of energy.

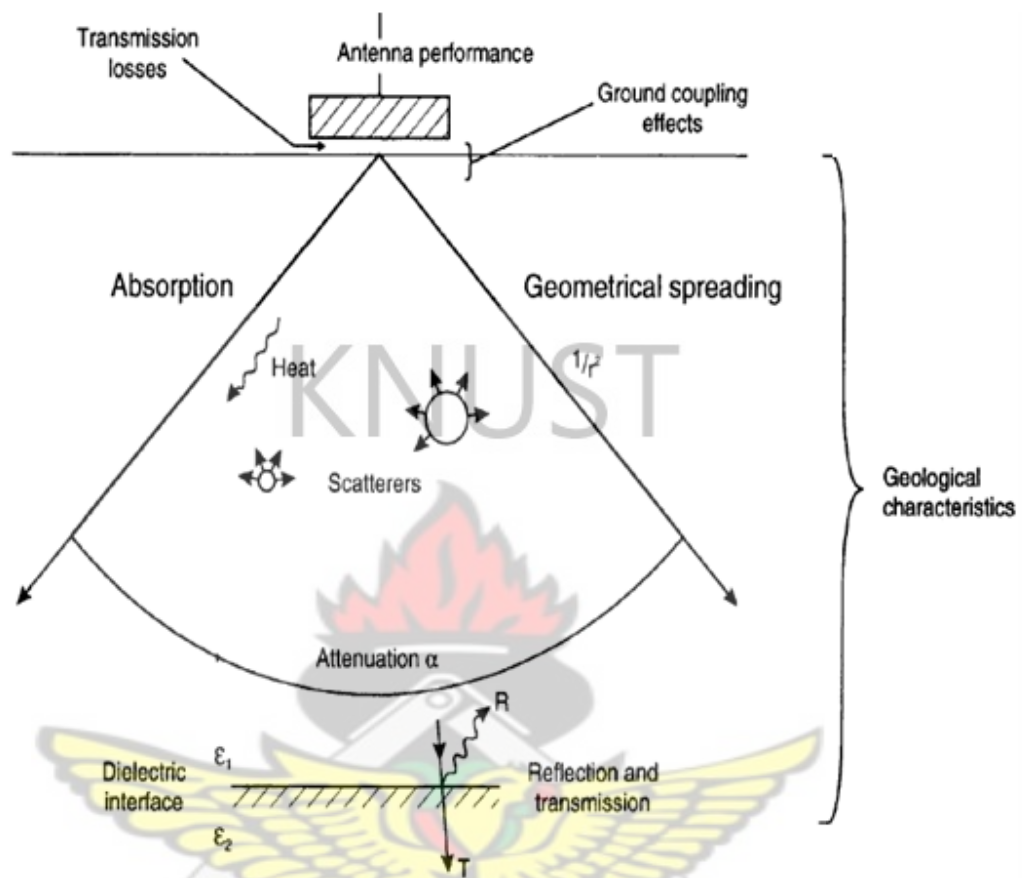


Fig. 2.2: Processes that lead to reduction in signal strength (Reynolds 1997).

Absorption, which is the conversion of electromagnetic energy into heat, is also another form of energy loss. Attenuation is another fundamental cause of loss of energy. It is a complex function of the dielectric and electrical properties of the media through which the radar is travelling. The depth by which the signal has decreased in amplitude to about 37% of the initial value is known as the skin depth (δ) and is inversely proportional to the attenuation factor. Figure 2.2 shows the processes that cause energy loss and attenuation.

Mathematical definitions of the attenuation are shown in Equations 2.14, 2.15, 2.116, 2.17.

$$\frac{E_x}{E_o} = \exp(-\alpha x) \dots \dots \dots (2.14)$$

where E_o is the peak electric field strength on transmission and at a distance x away E_x , α is the attenuation coefficient.

$$\therefore \alpha = \omega \left\{ \left(\frac{\mu \varepsilon}{2} \right) \left[\left(1 + \frac{\sigma^2}{\omega^2 \varepsilon^2} \right)^{\frac{1}{2}} - 1 \right] \right\}^{\frac{1}{2}} \dots \dots \dots (2.15)$$

$\omega = 2\pi f$, f is the frequency (Hz), μ is the magnetic permeability $\left(\frac{H}{m}\right)$,

σ is the bulk conductivity at a given frequency $\left(\frac{S}{m}\right)$,

ε is the dielectric permittivity $\left(\frac{F}{m}\right)$

$$\text{Also, Skin depth } (\delta) = \frac{1}{\alpha} \dots \dots \dots (2.16)$$

$$\text{Numerically, } \delta = (5.31\sqrt{\varepsilon_r})/\sigma \dots \dots \dots (2.17)$$

where ε_r is the bulk relative dielectric permittivity, and σ is in mS/m .

Skin depth is not synonymous with the depth of penetration of the ground radar. For an accurate assessment of the depth of penetration of ground radar, the loss of signal strength through the ground is most significant but the losses in the links between transmitters and receivers and their respective aerials and due to the directional characteristics of the aerials can also be significant. If the sum in dB of all instrumental factors is equal to F , then the radar range equation is represented in equation 2.18.

$$F = -10 \cdot \log_{10} [A\lambda^2 e^{-4\alpha r} / 16\pi^2 r^4] \dots \dots \dots (2.18)$$

where λ is the radar wavelength, α is the attenuation coefficient,

A is a shape factor and r is the theoretical maximum depth.

This equation determines how far in depth ground radar can go. The general model for assessing radar suitability by the radar range equation is given in Annan and Davis (1977). The equation cannot be solved directly for the range r , which appears in both the exponent and the divisor. Numerical models do however estimate ranges for different geological materials. A rough rule which is often applied where attenuation is known is that the depth of investigation will be less than 30 divided by attenuation (Milsom, 2003).

It has been shown in equation 2.15 that attenuation is directly proportional to frequency. The greater the frequency the higher the degree of attenuation. Other factors that can be seen to affect attenuation are bulk relative permittivity (ϵ_r), and bulk conductivity (σ) at the given frequency. Each of these properties is affected by the composition of the material and the electrical behaviour and relative abundance of each material constituent. The loss factor is directly proportional to the conductivity (σ) and inversely proportional to the relative permittivity (ϵ_r) and frequency. The more conductive any saturating fluid and the greater the proportion of fluid present with a correspondingly high relative permittivity, the greater will be the attenuation. Similarly, the greater the clay content, the greater the loss factor and hence the greater the attenuation.

2.1.5 Resolution

Vertical and horizontal resolutions both apply in GPR measurements. Vertical resolution is a measure of the ability to differentiate between two signals adjacent to each other in time. Vertical resolution is a function of frequency. Radar methods use the reflections of short bursts of electromagnetic energy (chirps) spanning a range of frequencies from about 50% below to 50% above some specified central frequency

(Milsom, 2003). Antennas are labelled with their centre frequency. The centre frequency is where the peak power occurs. That is, a 25 MHz antenna has a centre frequency of 25 MHz and a 50 MHz antenna has a centre frequency of 50 MHz. When GPR antennas are selected, the centre frequency is usually the most important parameter, since it, in practice, defines the resolution and the depth penetration of the radar signal. The bandwidth is equally important but less often referred to. The bandwidth is defined as the frequency span between two points. Daniels, Gunton and Scott (1988) noted that horizontal resolution is inversely proportional to $\sqrt{\alpha}$, where α is the attenuation coefficient.

2.1.6 Dielectric Properties of Geological Materials

Dielectric behaviour of a material is described in terms of its complex permittivity (ϵ^*) and complex conductivity (σ^*) which are interrelated (Equations 2.19, 2.20, and 2.21). Complex permittivity (ϵ^*) of a non-conductive material is given by,

$$\epsilon^* = \epsilon' + i\epsilon'' \dots \dots \dots (2.19)$$

If the material has conductivity σ , then,

$$\epsilon^* = \epsilon' + i(\epsilon'' + \sigma_s/\omega\epsilon_0) \dots \dots \dots (2.20)$$

where σ_s is the static or DC conductivity, and ϵ_0 is the permittivity of free space.

The complex conductivity σ^* is given by,

$$\sigma^* = \sigma' + i\sigma'' = j\omega\epsilon_0\epsilon^* \dots \dots \dots (2.21)$$

Relative permittivity (ϵ_r) varies from 1 in air through to 81 in water. For most geological materials ϵ_r lies in the range 3-30. Consequently, the range of radiowave velocities is large from around 0.06 m/ns to 0.175 m/ns. In trying to estimate depths to subsurface features, it is important to have a detailed knowledge of the radiowave velocities through the subsurface materials present.

2.1.7 Mode of Data Acquisition

Radar systems can be deployed in 3 modes. Reflection profiling (using either monostatic or bistatic antennas), wide angle reflection and refraction (WARR), or common-midpoint (CMP) sounding and transillumination or radar tomography.

2.1.8 Interference in GPR Surveys

Even when depth penetration, reflectivity and resolution seem satisfactory, environmental problems can prevent success in a GPR survey. Potential sources of interference are radio signals, mobile phones and metal objects (if they are not the survey targets).

2.1.9 Data Processing

Most of the processing tools used in GPR were appropriated from the processing of seismic data. GPR data processing has been extensively treated in Sensors and Software Inc report (1999). Fisher, et al. (1992), Maijala (1992) and Rees and Glover (1992) have all shown that while not all seismic processing methods can be applied to GPR data, a vast majority of the processing methods can be applied. As a rule of thumb, it is advisable to keep the filter settings as broadband as possible. From Reynolds (1997) the degree of processing is often determined by (a) the budget available; (b) the time available; (c) data quality; (d) the available processing capability (software and hardware); (e) the requirement that the final interpretation justifies further analysis; (f) the structural detail on the raw record meriting detailed quantitative data processing. Processing algorithms available are “de-wowing”, gain, background removal, bandpass filtering, different migration algorithms such as stolt, Kirchoff and the simple diffraction stack. Topographical correction can also be applied.

2.2 Impact Craters

2.2.1 Significance of Impact Craters

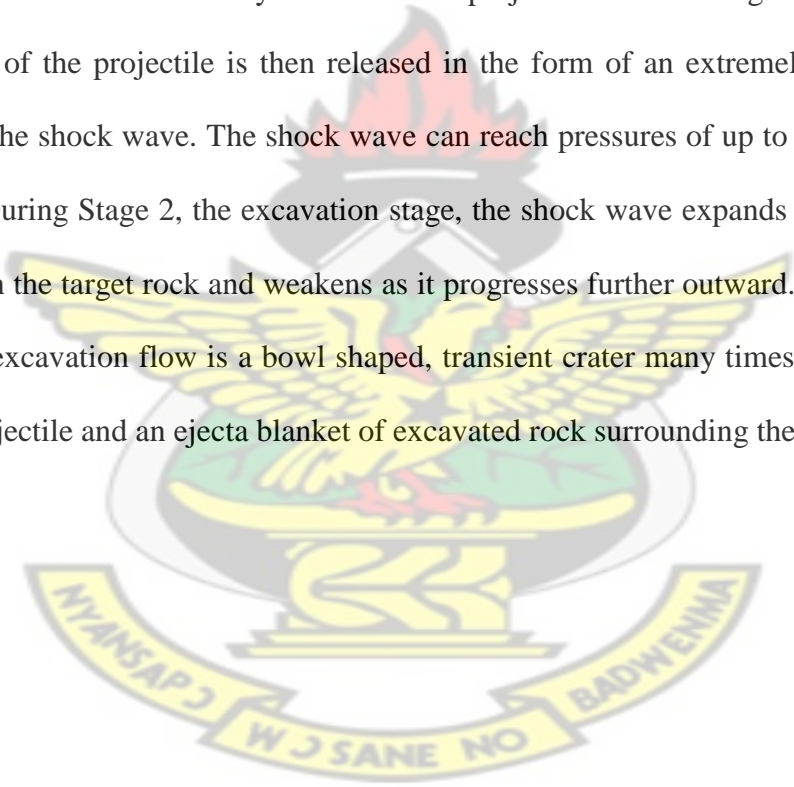
To date there are 182 confirmed impact structures around the world (Planetary and Space Science Centre, 2012). On earth however, geological and atmospheric processes tend to erase the impact record. The rate of impacts over the past 3.5 Ga has been roughly constant (Neukem, et. al 2001). Impacts have been observed in recent times as with the impact of Shoemaker-Levy 9 into Jupiter in 1994 (Roulston and Ahrens, 1997) and the Carancas cratering event in Peru in 2007 (Kenkmann et al., 2009). Impact craters are said to have caused geological and biological evolution on Earth (Koeberl and MacLeod, 2002) and even small impacts can disrupt the biosphere and lead to local and regional devastation of the living and non living things (Chapman and Morrison, 1994). Their predominance and effects have led Stöffler and Langenhorst (1994) to draw the conclusion that impact cratering has been a fundamental geologic process since the formation of the solar system and Shoemaker (1976) to state that impact cratering has been the most fundamental process that has taken place on terrestrial planets.

The significance of impact craters is therefore manifold. They serve as natural resource deposits as in one of the world's largest reservoirs of nickel and metal ores in the Sudbury impact structure in Ontario, Canada (Dressler, et al. 1987); and as in hydrocarbon resevoirs in the Chicxulub and Ames structures (Curtiss and Wavrek 1998). Another example of their significance is that their size-frequency distribution is used in dating planetary bodies (Neukem, et. al 2001). An example is the geological timescale on the moon which is based on cratering events (Stöffler and Ryder, 2001). Impact craters can also indicate paleoclimate change, an example being the work done on Mars (Boyce and Mouginis-Mark, 2006).

2.2.2 The Impact Cratering Process

Impacts on planetary surfaces occur at hypervelocities of tens of kilometres per second and on earth in particular, the average impact velocity is estimated to be at approximately 17 km/s (Poelchau, 2010). The impact cratering process is drawn from Gault (1968), Melosh (1989) and Poelchau (2010). There are three stages in the impact cratering process; contact and compression, excavation and modification. The impact process is divided into three stages based on the dominance of different physical phenomena at different times of the process (Gault 1968; Melosh 1989).

Stage 1 is characterized by contact of the projectile with the target surface. Kinetic energy of the projectile is then released in the form of an extremely high pressure pulse, the shock wave. The shock wave can reach pressures of up to several hundred GPa. During Stage 2, the excavation stage, the shock wave expands hemispherically through the target rock and weakens as it progresses further outward. The final result of the excavation flow is a bowl shaped, transient crater many times the diameter of the projectile and an ejecta blanket of excavated rock surrounding the crater.



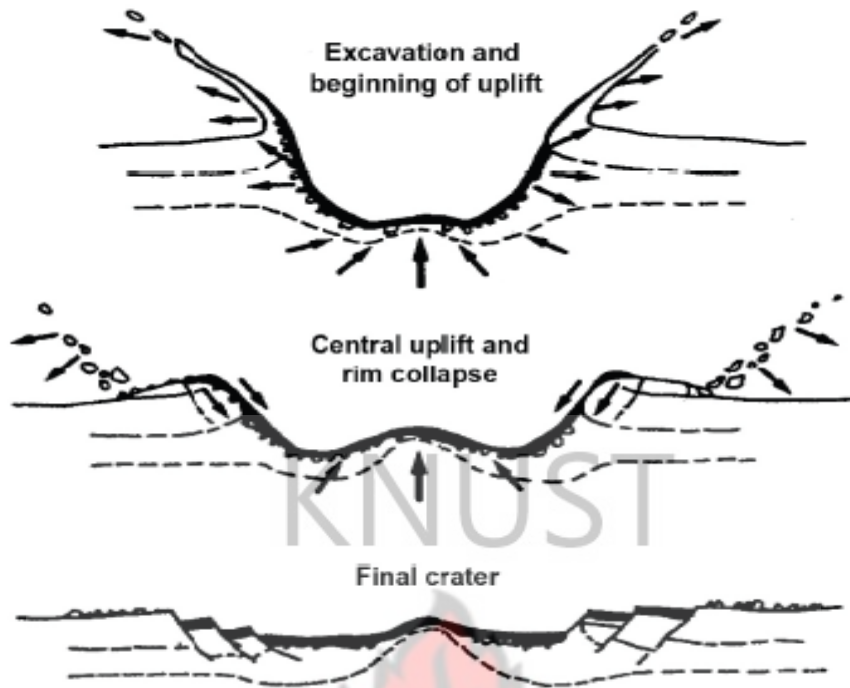


Fig. 2.3: Simplified sketches of the excavation and modification stages during the formation of a complex impact crater (Melosh, 1989).

Effects of the shock wave on the target are plastically deforming the medium and can even melt or vaporize the affected material after unloading. The duration of the pressure pulse is dictated by the projectile diameter.

At the final stage, the modification stage, the transient crater begins to collapse under the force of gravity. In craters greater than 4 km the crater walls slump inward to form radial terraces while a central uplift forms as the crater floor rises, forming what is called a complex crater. The stages are shown in figure 2.3.

2.2.3 GPR Investigations in Crater Terrains

The application of GPR in crater terrains investigations is limited. Work has however been done by Greeley, et al. (1987); Garvin, et al. (1989) and Grant, et al. (1995). In investigations carried out by Heggy and Paillou (2006), the sections are characterized by chaotic and perturbed bedrock as shown in figure 2.4.

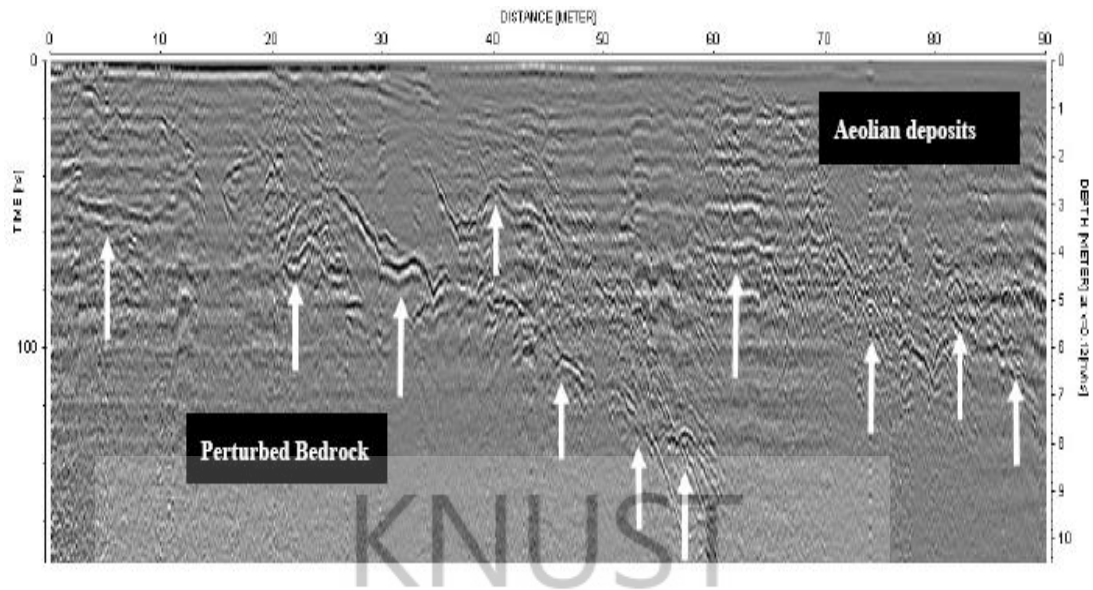


Fig. 2.4: Extract of a radar sounding (Heggy and Paillou 2006).

2.3 Geological Overview of the Bosumtwe Impact Crater

Geological studies have been going on in the Bosumtwe crater from the 1930's and these have led to a wide store of knowledge on the area. Work done by, Boamah and Koeberl (2003); Reimold, et al. (1998); Jones, et al. (1981); Moon and Mason (1967); and Junner (1937), have all focused on defining the geological framework of the Bosumtwe impact crater.

Intrusions of granitic-granodioritic bodies belonging to the Pepiakese and Kumasi group cross the Birimian Supergroup and Tarkwaian Supergroup stratas. The Tarkwaian Supergroup is actually said to be the detritus of and overlays the Birimian Supergroup. A variety of mafic and ultramafic intrusives also occur locally. In addition to these, rock formations that originated from the origins of the crater (impact breccias) and from weathering also occur in the area.

2.3.1 The Birimian Supergroup

Studies of the crater area have shown that the impact event excavated lower greenschist facies metasediments of the 2.1-2.2 Ga Birimian Supergroup. Even

though there are generally different kinds of rocks forming the Birimian Supergroup, the more important ones in the study area are mica schists and banded schists with both micaceous and quartz-feldspathic bands. Brecciated greywacke and phyllite dominate the geology immediately around the crater. They are locally intruded by small dikes and pods of granitic intrusive. Even with the dominance of the greywacke, drilling has revealed that shales are a major component of the target rocks. The area immediately around the crater rim is strongly deformed based on the study of road cuts and the crater rim zone has been subjected to impact induced faulting as well as folding (Reimold, et al. 1998).

2.3.2 The Tarkwaian Supergroup

Overlying the Birimian Supergroup is the Tarkwaian Supergroup. They are regarded as detritus deposited in the course of erosion of the Birimian strata. The Tarkwaian Supergroup includes phyllites, sandstone, quartzite, grits, breccias and conglomerate.

2.3.3 Dikes and Intrusives

Observations by Junner (1937); Woodfield (1966); Moon and Mason (1967); Jones (1985a); and Reimold, et al. (1998) are that several granitic intrusions of Proterozoic age occur in the region of the crater and some partially strongly weathered granitic intrusions (dikes) are present. A larger granitoid complex known as the Pekiakese occurs at the northeastern edge of the crater. Mafic intrusives have also been observed in the environs of the crater.

2.3.4 Breccia

Occurring in the region of the crater are also breccia exposures. It is however unclear whether all these breccias represent impact breccias (Reimold, et al. 1998). It has been speculated by Koeberl and Reimold (2005) that at least some of the breccias

may be as a result of lateritization and secondary mass wasting.

A detailed structural analysis of the crater by Reimold, et al. (1998), showed that the area immediately around the lake in the inner crater is characterized by inward dipping shear zones and faults (figure 2.5). Toward the lowestmost inner part of the rim, blocks of all regional lithologies are highly fractured and sheared and locally internally brecciated. Figure 2.6 shows a general geological map of the Bosumtwe impact crater and its environs.

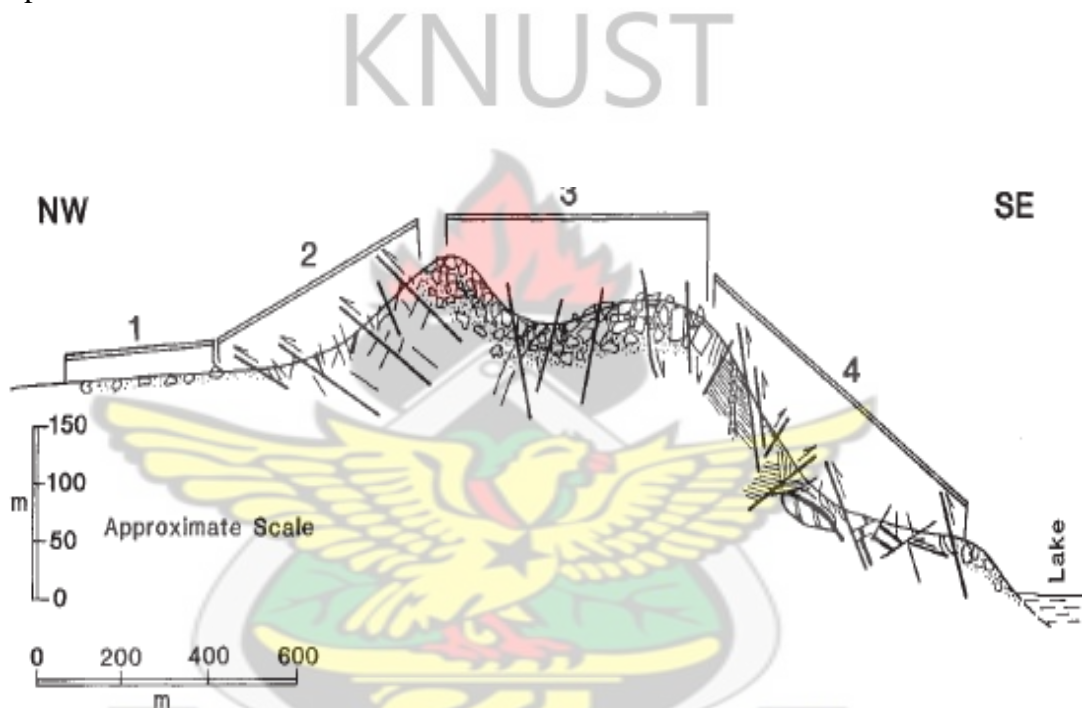


Fig. 2.5: Zonation of northwestern crater rim. Zone 1: dominantly ejecta breccias cover and local mass wasting. Zone 2: inward dipping thrust planes, conjugate radial fractures, isoclinal folding, and overturned stratigraphy. Zone 3: megabreccia with upward decreasing block sizes. Zone 4: dominant thrust faulting of multiple orientations, resulting in duplex and lens shaped bodies of pre-impact strata (Reimold, et al.).

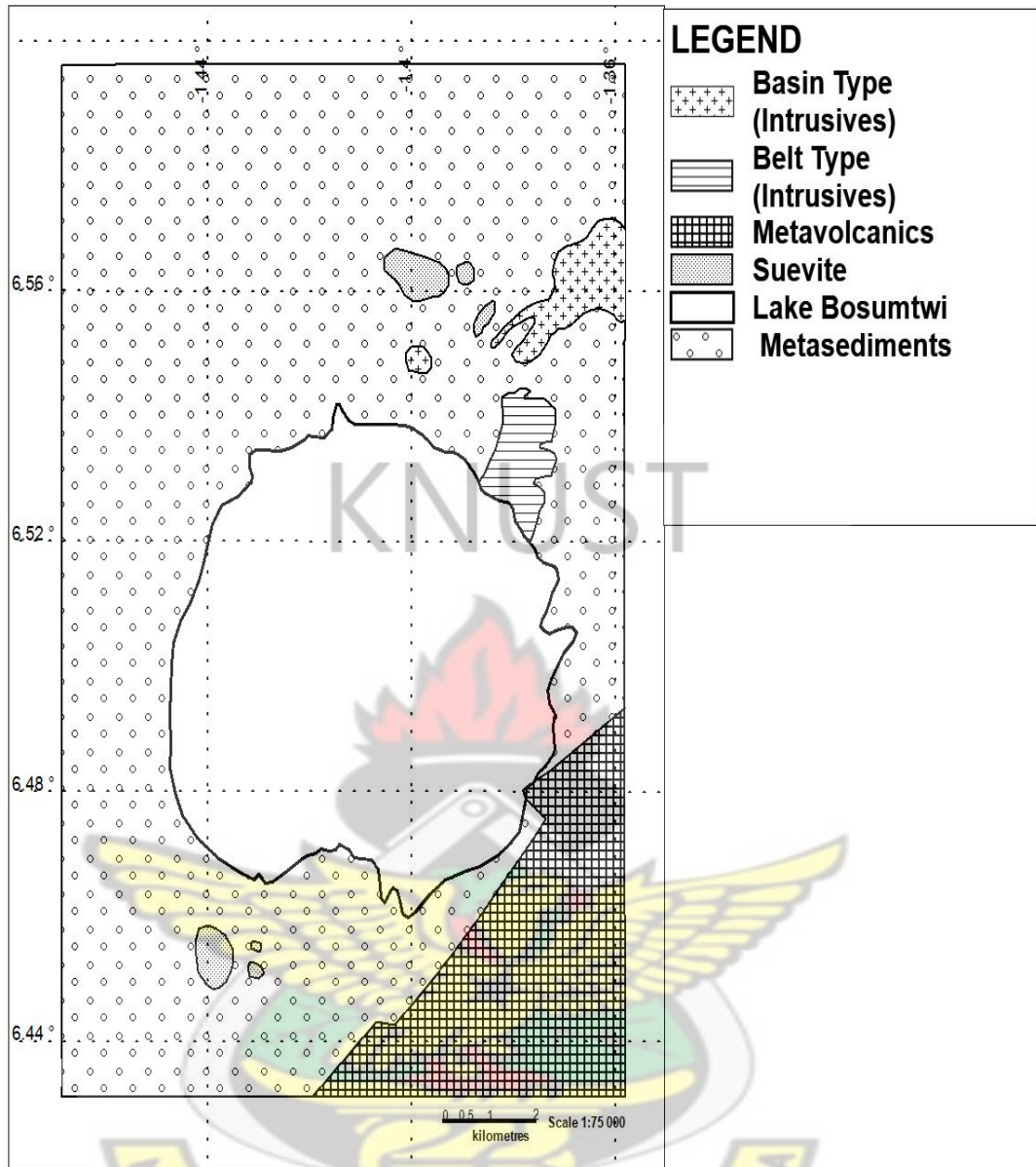


Figure 2.6: Geological Map of the Bosumtwi Impact Crater (Modified from Koeberl and Reimold, 2005).

CHAPTER THREE

MATERIALS AND METHODS

3.0 Materials and Methods

3.1 GPR Equipment

The Mala GPR system was used for conducting the survey. Specifications of the system were gathered from Mala Geoscience (2012). The system includes the Mala XV monitor, the Mala ProEx system and the Mala Rough Terrain Antenna (RTA). A Mala XV monitor is a dedicated data acquisition platform with a unique user interface and is based on the Mala ProEx system. The Mala rough terrain antenna (RTA) is also based on the ProEx system and uniquely designed for low frequency surveying. It is an unshielded antenna which is snakelike. All the components are shown in figure 3.1.



Fig. 3.1: The Mala GPR system used for the survey

3.2 Data Acquisition

20 GPR profiles were taken across the northern section of the inner morphological crater. All the profiles were above the 6°30'N latitude. Two sets of profiles were taken: Profile 1 to 12 (perpendicular to the lakeshore at initial point) and Profile 15 to 22 (parallel to the lake shore at initial point). The GPS location of the initial point of both sets of profiles were plotted in Golden Software Surfer using the UTM coordinates. The Bosumtwé crater can be found in UTM Zone 30. This is shown in figure 3.2.

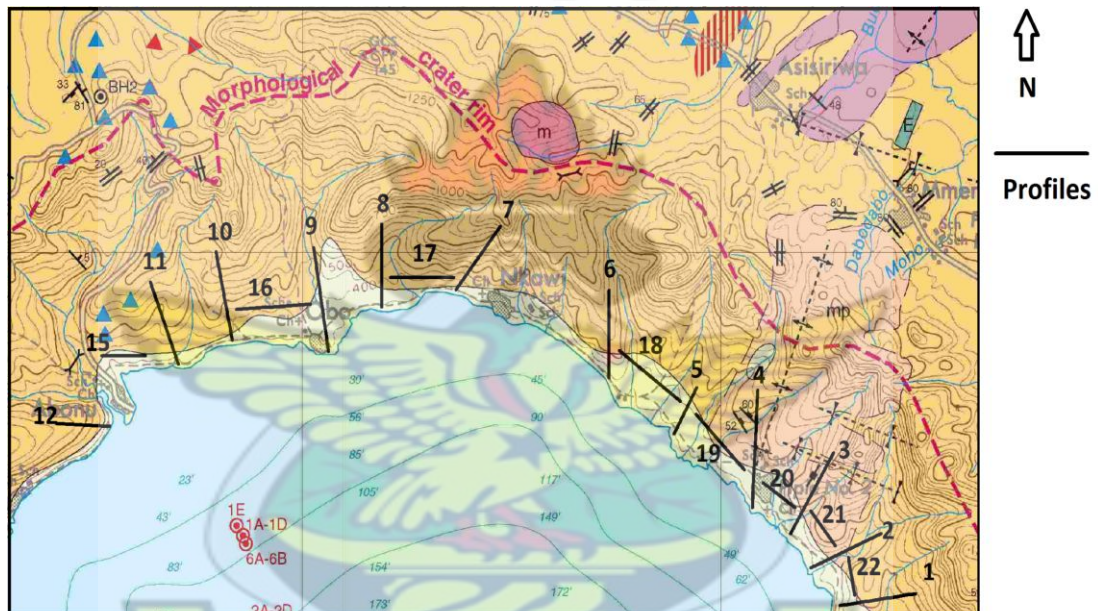


Fig. 3.2: Locations of profiles.

GPS locations of the profiles are in Appendix 1. The Garmin handheld GPS was used to mark GPS locations. The lengths of profiles were dependent on the ability of the survey team to navigate the slopes and dense vegetation cover. Profile names, lengths of profiles and direction are shown in Table 3.1.

The GPR equipment was used in bistatic mode configuration with central frequencies of 25 MHz and 50 MHz.

Table 3.1: Profile names, lengths and directions.

Profile Name	Length of Profile	Direction
1	400	SW-NE
2	200	SW-NE
3	400	SW-NE
4	500	S-N
5	150	SW-NW
6	400	S-N
7	300	SW-NE
8	400	S-N
9	400	S-N
10	270	SE-NW
11	320	SE-NW
12	200	SE-NW
15	120	SW-NE
16	840	SW-NE
17	700	W-E

Profile Name	Length of Profile	Direction
18	580	NW-SE
19	600	N-S
20	650	NW-SE
21	600	NW-SE
22	500	W-E

It is observed from Table 3.1 that some of the profiles (Profiles 1, 2, 3, 7, 15 and 16) even though in categories, went in the same direction. This is due to the uneven nature of the shore and the fact that the survey team used the easily accessible paths in defining profile direction. Two prospecting frequencies of 50 MHz and 25 MHz (Rough Terrain Antenna) were used over the same profiles in order to adequately resolve different depths.

The time triggering mode was used. Table 3.2 shows the acquisition parameters for the GPR survey. The GPR survey was conducted with a 4-person team over a 5-day period. Continuous coverage was achieved over the profile by using the common offset method. The Rough Terrain Antennas (RTA) were pulled manually. Images from the data acquisition stage of the project can be seen in figure 3.3.

3.3 Data Processing

The digital data gathered was processed using Sandmeier's Reflex-Win software. The first step in the filtering process is usually temporal filtering. This is done to remove low frequency components of the data and it is known as "dewowing". Very

low frequency components of the data are associated with either inductive phenomena or possible instrumentation dynamic range limitations (Sensors and Software Inc, 1999).

Table 3.2: Acquisition parameters of GPR survey

	Central frequencies	
	25 MHz	50 MHz
1. Antenna spacing	6.2 m	4.2 m
2. Sampling frequency	250	500
3. Maximum depth of penetration	39 m	61 m
4. Measuring mode	Continuous	
5. Antenna orientation	Inline configuration	

Static correction was used to get rid of the time delay. The time-delay occurs because a GPR system generally does not know the exact time when the transmitter fires, therefore a reference in the data must be used to work backwards to find the true time-zero. The reference used is the arrival of the direct wave. AGC (automatic gain control) filter was applied to enhance signals from deeper underground and for stratigraphic horizon continuity. To eliminate horizontal stripes on the radargram, a background removal was applied.

Different migration algorithms based on constant velocity models were applied and compared, to note the quality of diffraction removal on the sections. Migration algorithms applied were diffraction stack, f-k filtering (Stolt) and Kirchoff migration.

An electromagnetic velocity of 0.11 m/ns was used for the migration. Finally a topographic correction was applied for Profile 1 to 12 which were taken across varying elevation positions.



Fig. 3.3: Images from data acquisition stage

CHAPTER FOUR

RESULTS AND INTERPRETATION

4.0 Results and Interpretation

4.1 Migration Algorithms

Results from the different migration algorithms are compared using 25 MHz sections from Profiles 1, 2, 18 and 21.

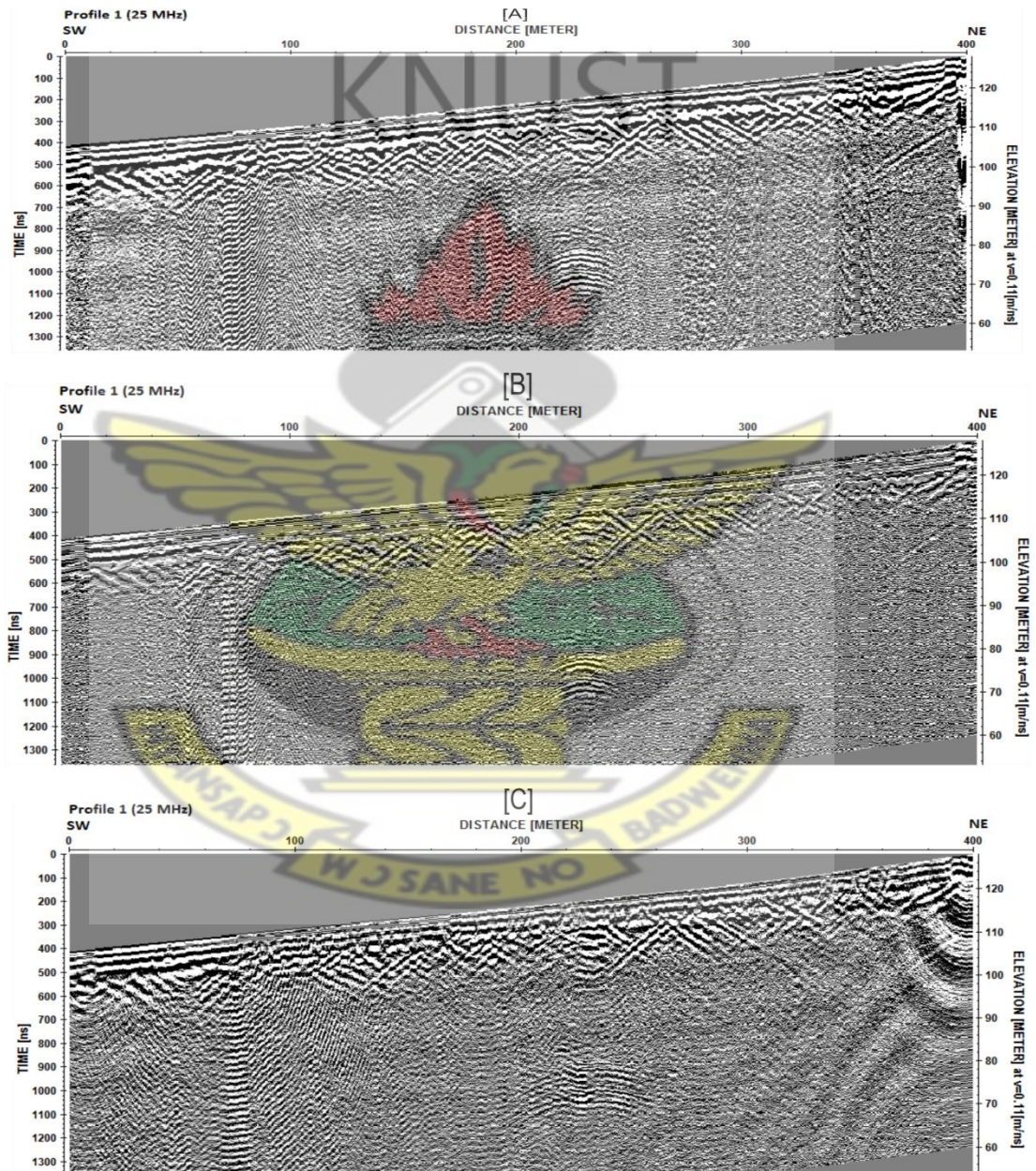


Fig. 4.1: Profile 1 obtained with the 25 MHz RTA and migrated with (A) diffraction stack algorithm (B) Kirchoff algorithm (C) f-k algorithm.

From the 25 MHz sections of Profile 1 in figure 4.1, it is clearly observed that the diffraction stack algorithm was the most successful in migrating subsurface features to their true depths and collapsing hyperbolas.

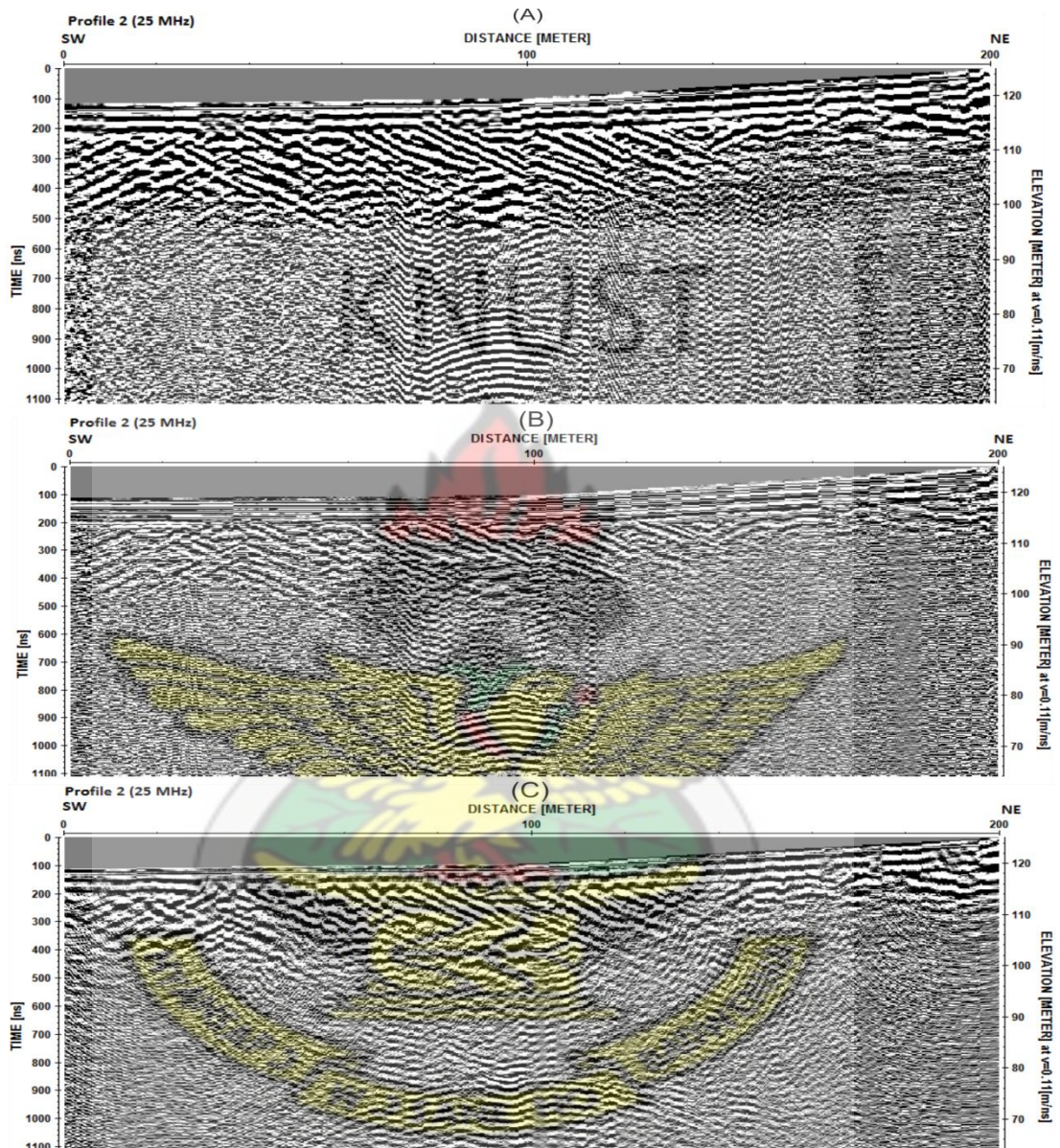


Fig. 4.2: Profile 2 obtained with the 25 MHz RTA and migrated with (A) diffraction stack algorithm (B) Kirchoff algorithm (C) f-k algorithm.

From the 25 MHz sections of Profile 2 in figure 4.2, it is clearly observed that the diffraction stack algorithm was the most successful in migrating subsurface features to their true depths and collapsing hyperbolas.

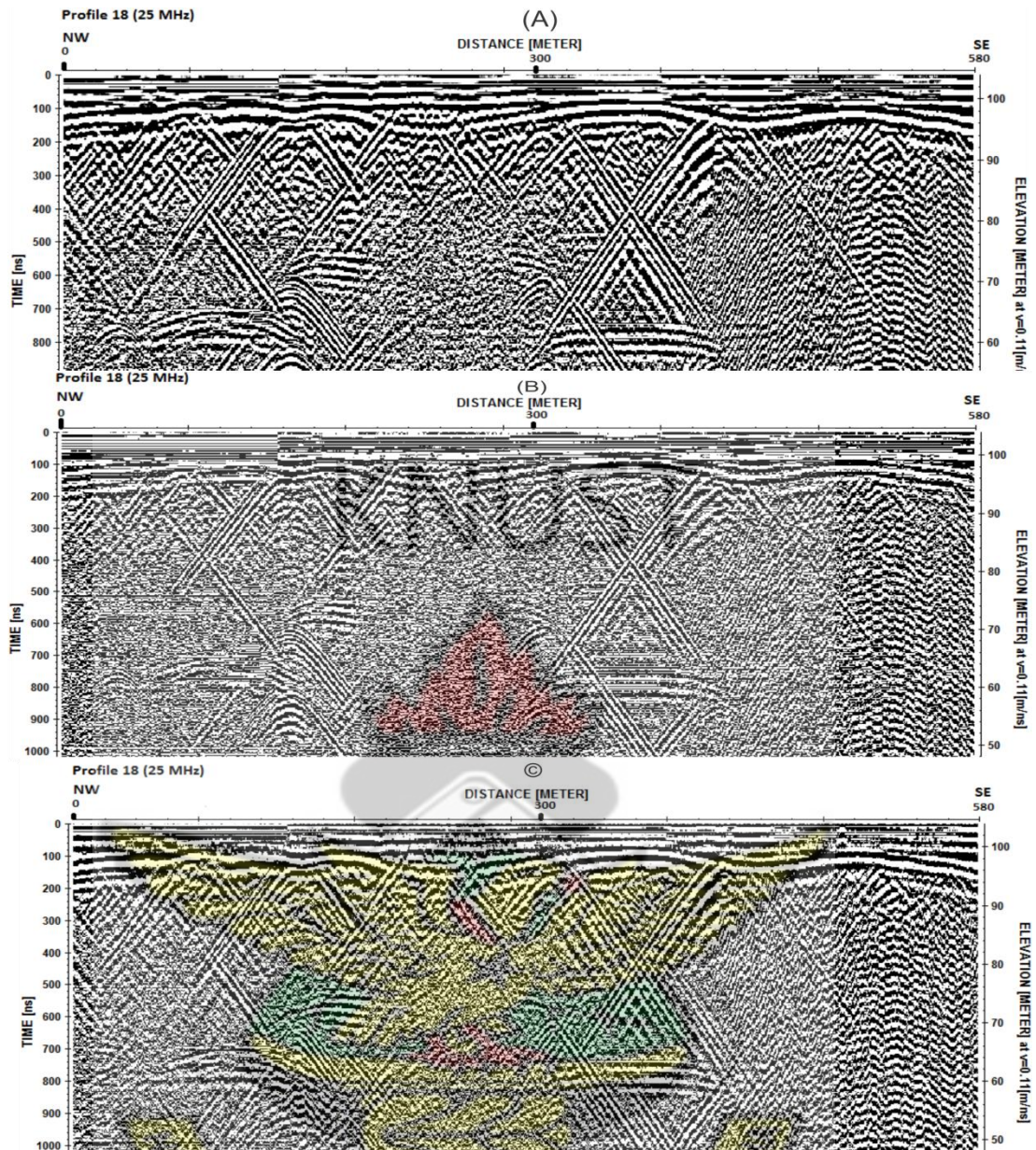


Fig. 4.3: Profile 18 obtained with the 25 MHz RTA and migrated with (A) diffraction stack algorithm (B) Kirchhoff algorithm (C) f-k algorithm.

From the 25 MHz sections of Profile 18 in figure 4.3, it is clearly observed that the diffraction stack algorithm was the most successful in migrating subsurface features to their true depths and collapsing hyperbolas.

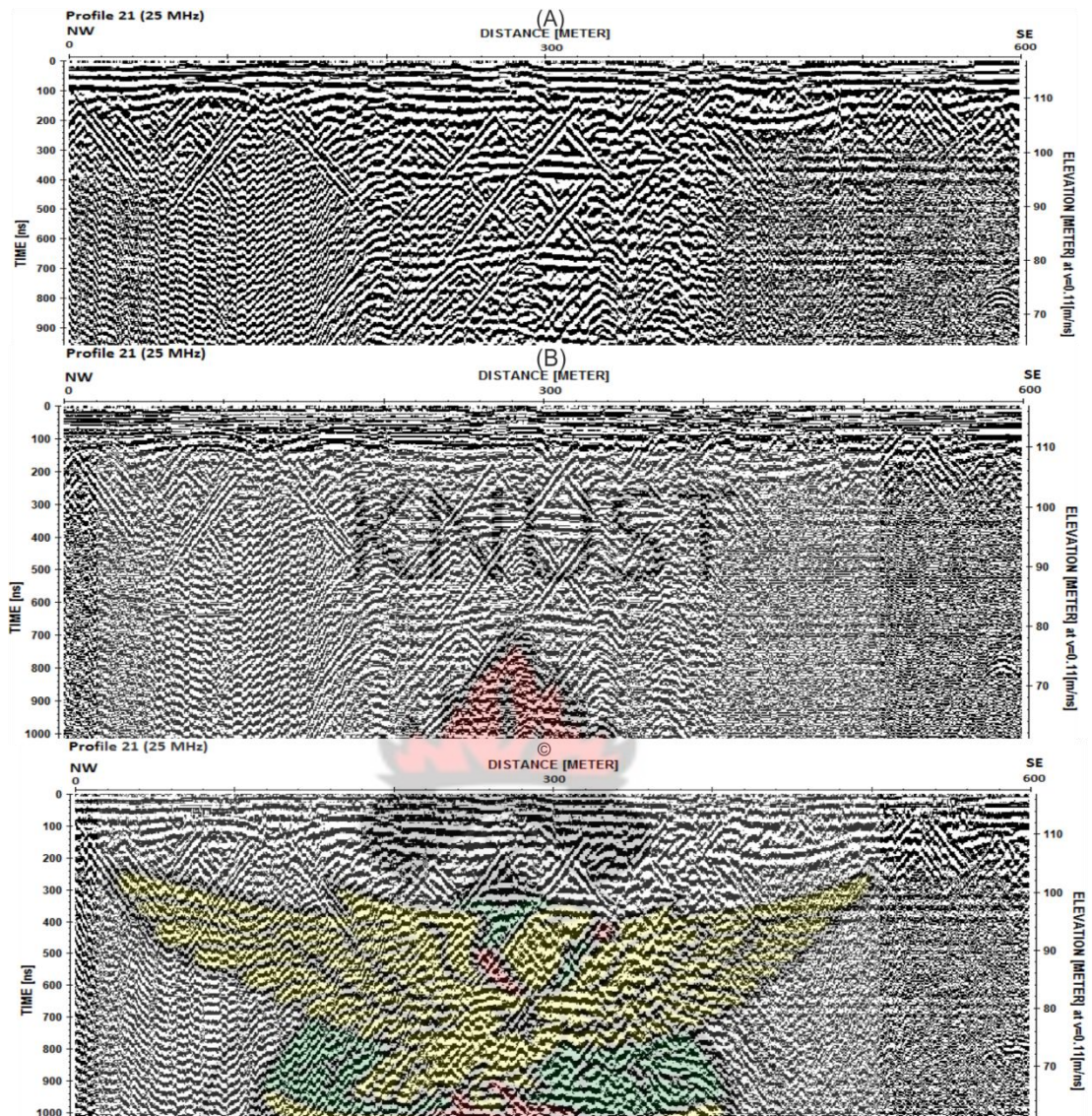


Fig. 4.4: Profile 21 obtained with the 25 MHz RTA and migrated with (A) diffraction stack algorithm (B) Kirchoff algorithm (C) f-k algorithm.

From the 25 MHz sections of Profile 21 in figure 4.4, it is clearly observed that the diffraction stack algorithm was the most successful in migrating subsurface features to their true depths and collapsing hyperbolas.

In all cases, the diffraction stack algorithm effectively collapsed the hyperbolas and migrated subsurface features to their true depths. Therefore the diffraction stack algorithm section was used for the results presented for all the profiles.

Radargrams from the 25 MHz and 50 MHz RTA were also compared. 25 MHz

sections and the 50 MHz sections of selected profiles (9 and 16) are compared to confirm the ability of the different central frequencies to resolve different depths. The diffraction stack migrated sections are used for the comparisons.

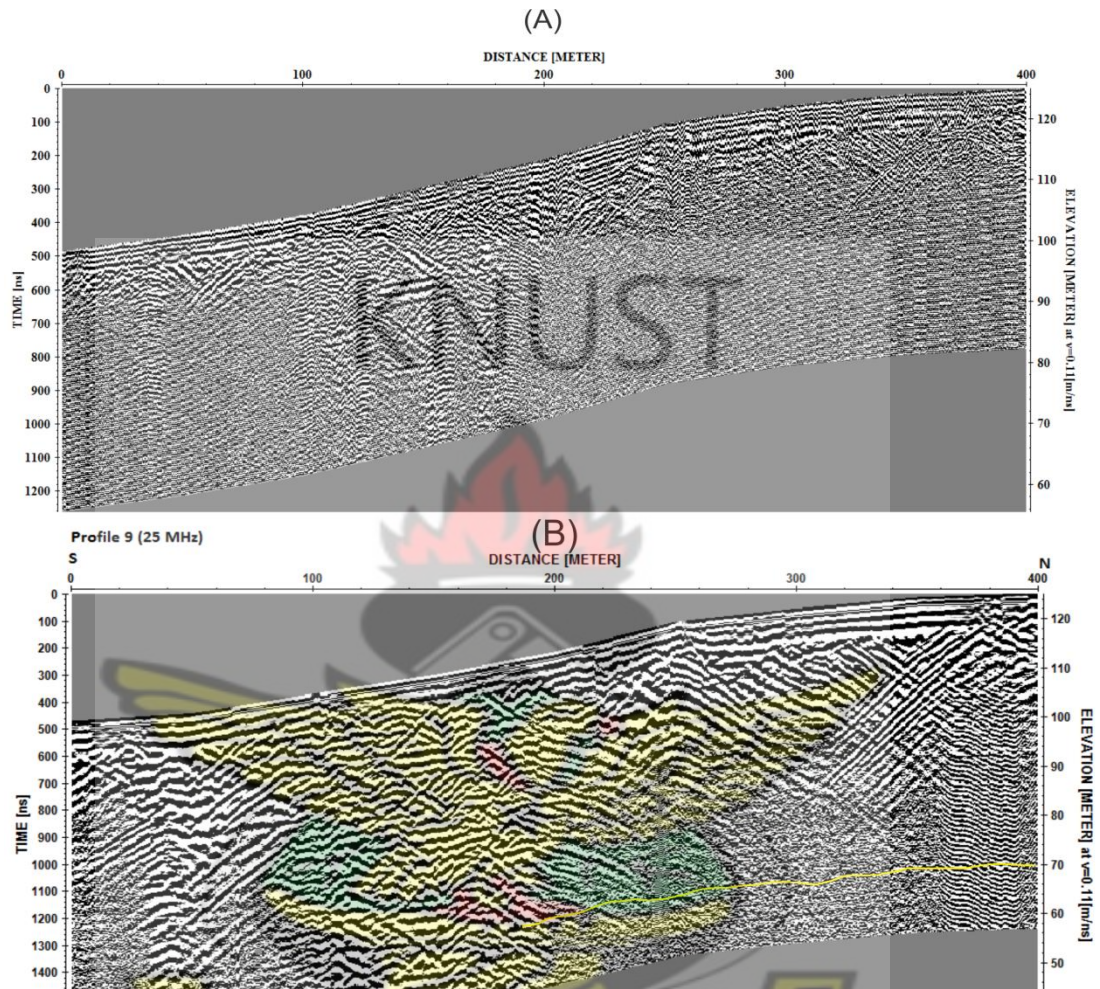


Fig. 4.5: Comparison of (A) 50 MHz and (B) 25 MHz sections of Profile 9.

In figure 4.5 it is observed that subsurface features that are at elevations of 70 m and below can be located on the 25 MHz section but are not present on the 50 MHz section.

In figure 4.6 the upper 17 m of the section is more clearly resolved on the 50 MHz section and the difference between the layers much clearer. Below the 116 m elevation however, the 50 MHz signal is rapidly attenuated. In the bottom right

corner of the 25 MHz section, a dipping layer interspersed with a hyperbola is observed at an elevation of 70 m. This subsurface feature cannot be observed on the 50 MHz section.

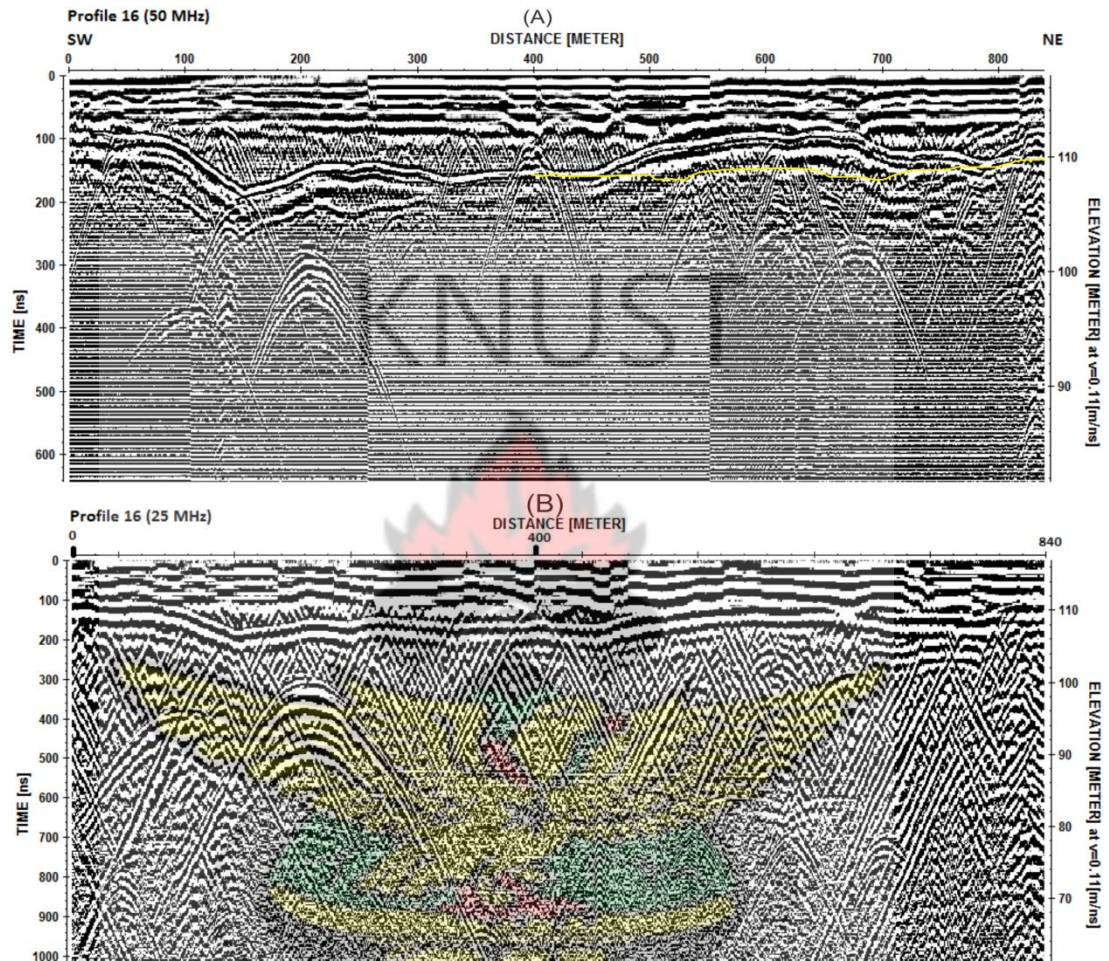


Fig. 4.6: Comparison of (A) 50 MHz and (B) 25 MHz sections of Profile 16.

The 50 MHz prospecting frequency ably resolved the upper 30 m while the 25 MHz resolved deeper features. The 25 MHz sections however effectively represent the target subsurface features at all depths so were used for identifying the target features.

4.2 Profile Sections

4.2.1 Profile 1

Figure 4.7 shows the anomalies identified on the section. Profile 1 has a length of 400 m. The direction of the profile is in the north-east direction. The profile has varied elevation from 105 m to 128 m. The upper 10 m of the immediate surface along the profile is characterized by multiple diffraction hyperbolas (below red layer). This is indicative of multiple fractures at the immediate subsurface or may also indicate obstructions such as trees in the profile path. A significant anomaly is also noted at a distance of 220 m along the profile (marked green). The elevation at the surface of the diffractive hyperbola anomaly is 80 m. This anomaly is indicative of the duplex or lens shaped bodies of pre-impact strata suggested by Reimold, Brandt and Koeberl (1998) to be present within the crater rim, a fracture within a subsurface layer. Another anomaly is a strong reflection layer along the entire profile length (indicated by red colour). This layer is about 6 m below the surface of the profile. It is suspected that this strong reflection layer is the layer of unconsolidated breccias from weathering. At the upper right corner of the section is a reflection layer at an elevation of between 100 m to 120 m (marked in blue). This feature is suggestive of a fracture at the subsurface. The fracture is oriented in the north-eastern direction.

4.2.2 Profile 2

Profile 2 (figure 4.8) begins from the lake shore and extends in the north-easterly direction for 200 m. Elevations along the profile vary from 118 m to 125 m. The most significant anomaly on the section is the diffraction at a distance of 100 m along the profile and an elevation of 80 m marked in green. It is suspected to be either an intrusive or a duplex or lens shaped bodies at the subsurface. The anomaly

marked in red on figure 4.8 suggests a perturbed bedrock which varies between elevations of 120 m to 100 m. The immediate subsurface (upper 16 m) is characterized by multiple diffractions indicative of unconsolidated breccia and loose rocks on the surface.

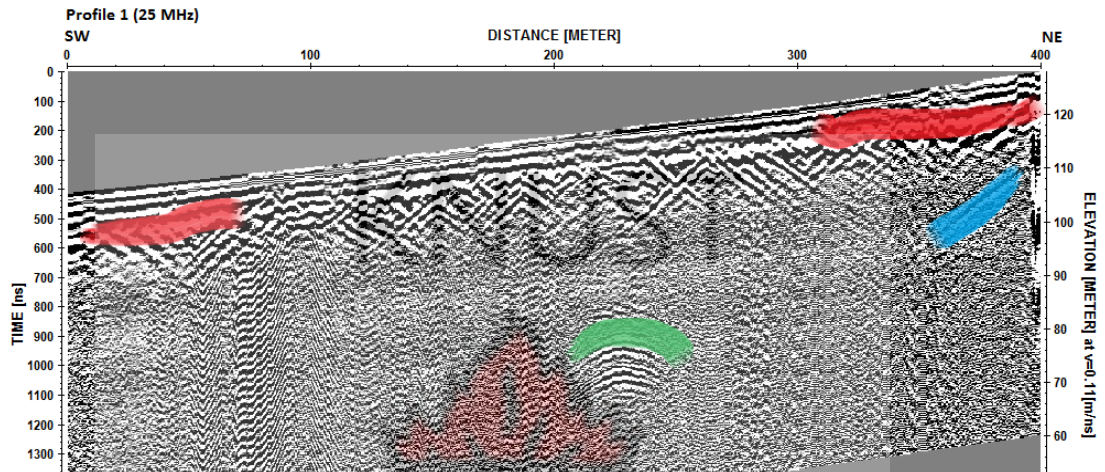


Fig. 4.7: Profile 1 showing marked anomalies.

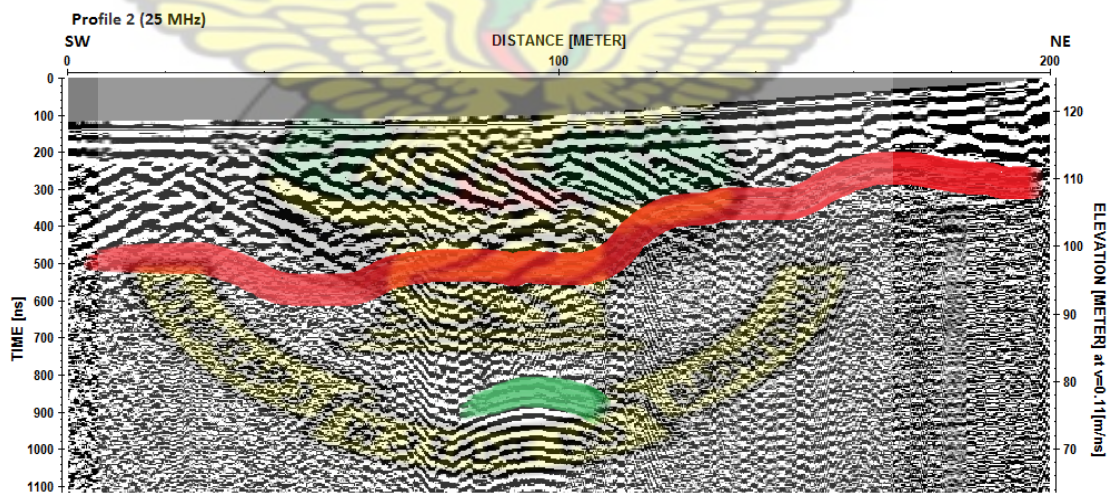


Fig. 4.8: Profile 2 showing marked anomalies.

4.2.3 Profile 3

Profile 3 (figure 4.9) is 400 m long and has elevation varying from 101 m at the shore to 124 m towards the rim of the crater. The general direction of the profile was in the north-eastern direction from the shore. The feature marked in red on figure 4.9

is a strong amplitude reflection surface that is interpreted to be the top layer of unconsolidated breccia. It lies 6 m from the surface of the profile and runs along the whole section. Another significant anomaly on the section is marked in green on figure 4.9. This is part of the perturbed bedrock between the elevations of 85 m to 100 m and extends from the beginning of the profile and disappears at a distance 180 m along the profile. Strong reflections can be found on the profile running from the top of the profile downwards. They are present across the immediate subsurface and can be found in the same vicinity as the multiple diffractions. They are marked in blue on figure 4.9. This feature on the section suggests multiple fractures oriented in different directions.

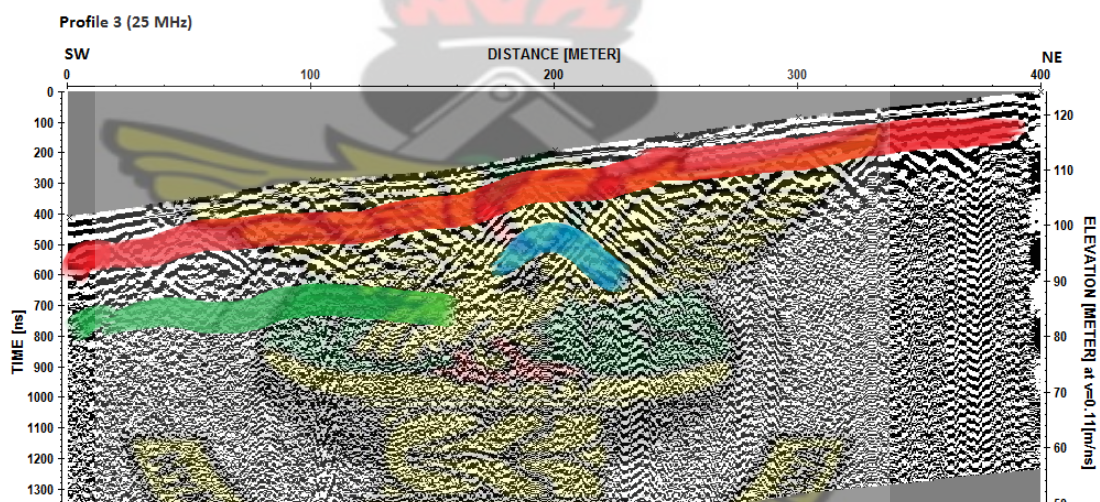


Fig. 4.9: Profile 3 showing marked anomalies.

4.2.4 Profile 4

The 25 MHz section of Profile 4 used for interpretation is shown in figure 4.10. Profile 4 is 500 m long and has elevations varying from 93 m at the shore of the lake to 132 m towards the crater rim. The profile is aligned in the south-north direction. The most prominent anomaly noted on the section is marked in red on figure 4.10. This anomaly is a strong amplitude reflection layer. It indicates the interface between

the unconsolidated breccias on the slope and the consolidated breccias underlying it.

This anomaly is present at a depth of 5 m.

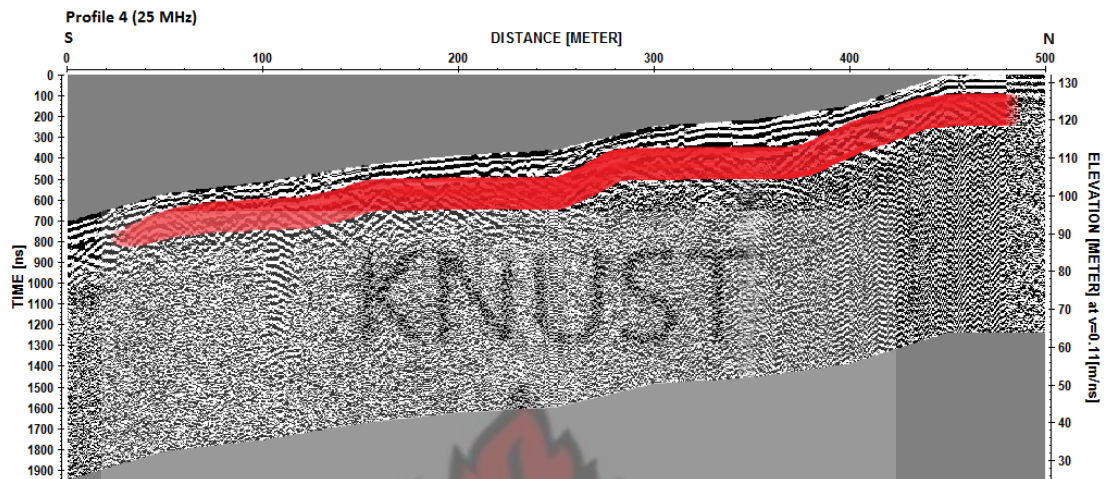


Fig. 4.10: Profile 4 showing marked anomaly.

4.2.5 Profile 5

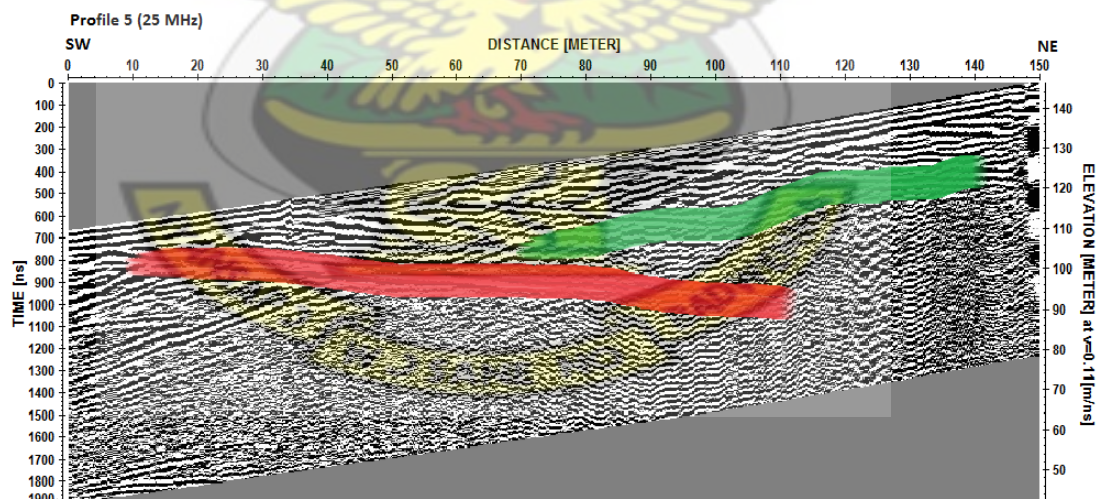


Fig. 4.11: Profile 5 showing marked anomalies.

The profile is 150 m long and has elevation varying from 109 m at the shore of the lake to 146 m towards the crater rim. The profile runs in the southwest-northeast direction. Anomalies are marked on figure 4.11. The most prominent anomaly on the

feature is marked in red on figure 4.11. It is a strong amplitude reflection that extends from 10 m to 120 m along the profile with an elevation varying from 90 m to 110 m. This anomaly is suggestive of a water table reflection. The anomaly marked in green is however diffractions suggestive of the unconsolidated breccia at the immediate subsurface. It is located at the upper 24 m of the subsurface.

4.2.6 Profile 6

Anomalies are labelled on a section of Profile 6 shown in figure 4.12. Profile 6 is 400 m long and elevation along the profile varies from 100 m at the shore of the lake to 174 m towards the rim of the crater. The profile extends from the shore of the lake in the northern direction. The upper 20 m of the subsurface is characterized by multiple diffractions which are indicative of the unconsolidated breccias (above the red label). The second significant anomaly on the section is a strong reflection layer between the elevations of 140 m and 120 m. It lies between 100 m and 270 m along the profile, truncates and continues from 340 m to the end of the profile. This layer is suggestive of a bedrock layer. The approximate depth to bedrock varies between 10 m to 40 on this section.

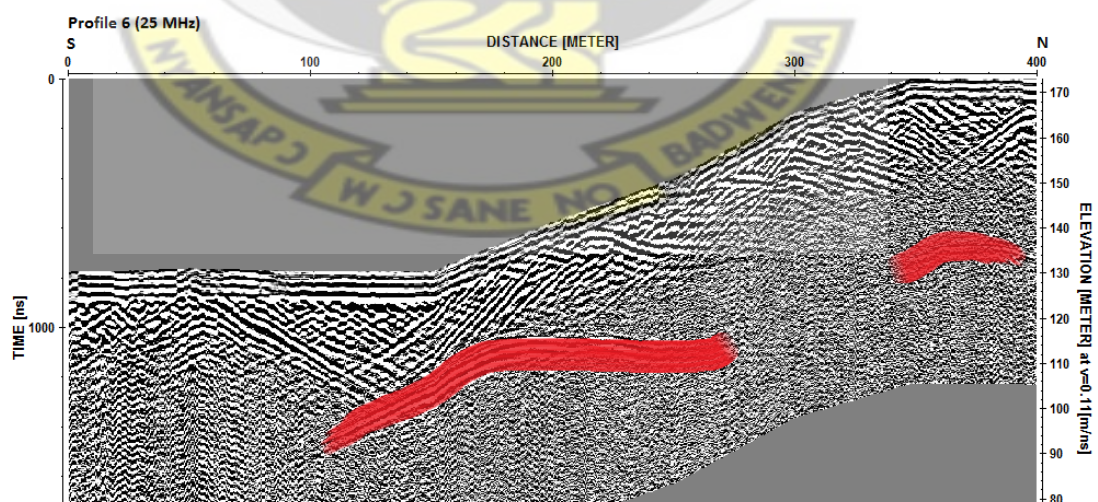


Fig. 4.12: Profile 6 showing marked anomalies.

4.2.7 Profile 7

Figure 4.13 shows the 25 MHz section taken of profile 7. Profile 7 is 300 m long and elevation along the profile varies from 118 m at the shore of the lake to 160 m towards the rim of the crater. The profile begins from the shore of the lake and extends in the north-eastern direction. Several significant anomalies are noted on the section. A strong reflection layer is seen running along the whole profile at the upper 6 m of the section. This anomaly is marked in red on figure 4.13. The anomaly is indicative of the unconsolidated breccia at the upper part of the subsurface created from weathering processes. This also causes the scattering of radar signals creating the multiple diffractions found in the upper 20 m of the section. Some of the diffractions are marked in green on figure 4.13. At an elevation of 80 m is a diffraction hyperbola marked in blue. This anomaly is suggestive of an intrusive, lens or duplex shaped bodies present in the subsurface.

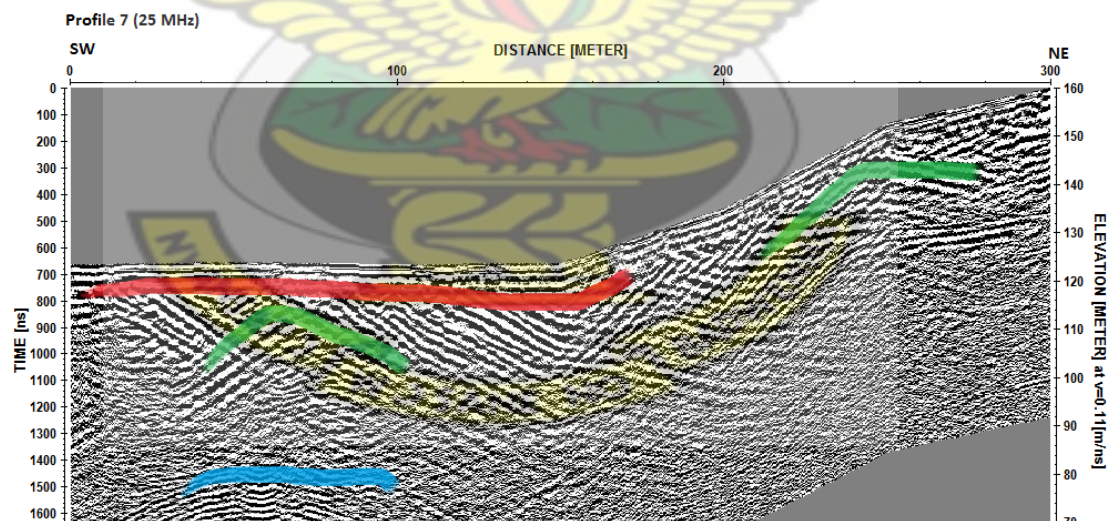


Fig. 4.13: Profile 7 showing marked anomalies.

4.2.8 Profile 8

Figure 4.14 is a 25 MHz section of Profile 8 showing marked anomalies. The length of Profile 8 is 400 m with variations in elevation between 110 m at the beginning of the profile to 146 m at the end of the profile. The profile extends from the shore of

the lake in a south-north direction. Profile 8 is characterised by three significant anomalies. Several diffractions characterise the immediate subsurface (upper 15 m). These diffractions are due to the presence of unconsolidated breccia along the slopes of the profile and are marked in green on figure 4.14. A strong amplitude reflection with discontinuities is present on the section and is marked in red. The reflection layer is between an elevation of 95 m and 130 m on the sections and is indicative of a perturbed bedrock. An interpretation of perturbed bedrock is reinforced by the breakages in the layer. Discontinuities in the layer are present from 60 m to 120 m, and from 160 m to 300 m along the profile. The discontinuities present on the section suggest fractures in the bedrock.

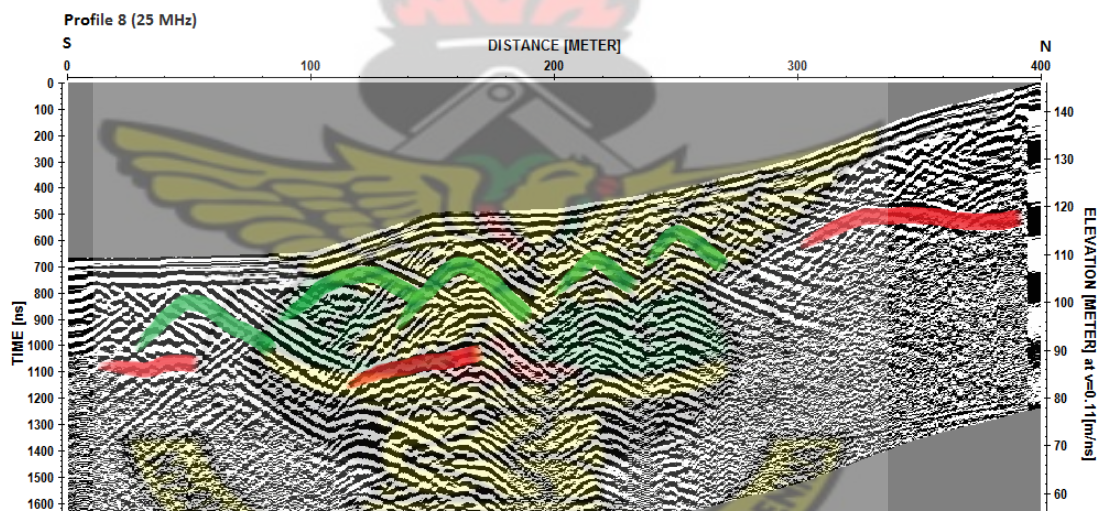


Fig. 4.14: Profile 8 showing marked anomalies.

4.2.9 Profile 9

Anomalies on the section for Profile 9 are shown on figure 4.15. The length of Profile 9 is 400 m. Elevation along the profile varies from 98 m at the shore of the lake to 125 m at the end of the profile. Profile 9 extends from the shore in the northern direction. Four anomalies are significant on the profile and are shown in figure 4.15. A strong reflection layer is seen running across the section from the

beginning to the end of the profile. This anomaly is marked in red. This layer is the boundary between the unconsolidated breccia and consolidated breccia along the profile surface. It is 5 m below the surface of the profile. Immediately below the reflection layer is a set of diffractions created on the section due to the presence of the unconsolidated breccias which scatter the radar signals. Some of these diffractions are marked in green on the section. Another prominent anomaly on the section is reflection layer that begins at a distance of 50 m along the profile breaks at about 100 m begins again at a distance of 120 m along the profile and terminates at a distance of 200 m. This layer is interpreted to be part of the perturbed bedrock. The discontinuities observed at a distance of 100 m and 200 m are assumed to be fractures.

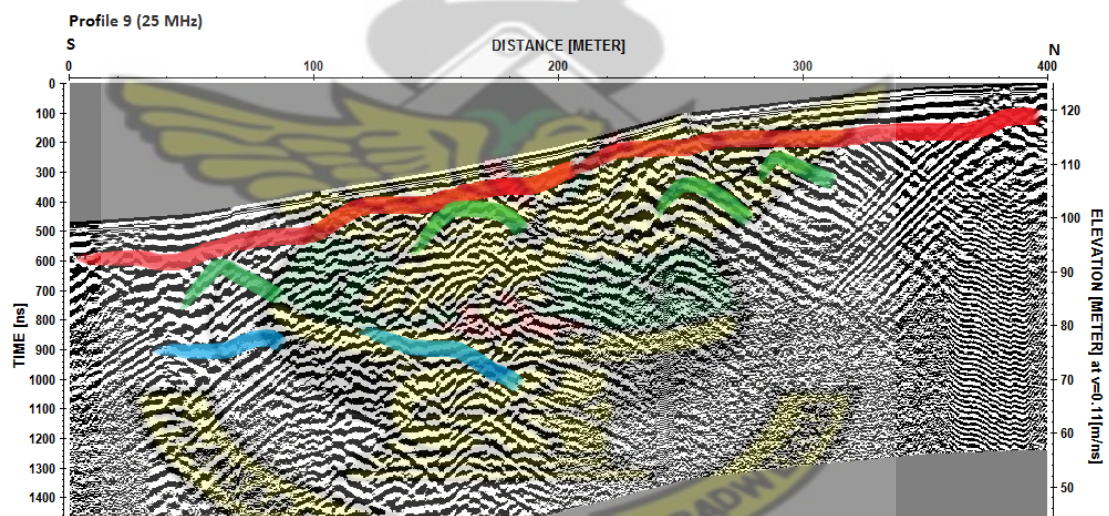


Fig. 4.15: Profile 9 showing marked anomalies.

4.2.10 Profile 10

The labelled section of profile 10 is shown in figure 4.16. Profile 10 is 270 m long and varies from an elevation of 108 m at the shore of the lake to 137 m at the end of the profile. The profile extended from the shore in the north-western direction. Prominent anomalies on the section are marked in red, green, blue and yellow. The

first of these is the strong reflection layer with discontinuities at various points marked in red. This layer begins from the beginning of the profile and is first broken at 40 m along the same profile. It then stretches again from 90 m to 110 m along the profile. The final section of this layer occurs at 160 m to the end of the profile. The layer falls within the elevation 100 m to 120 m. The structure is interpreted to be part of the perturbed bedrock characterised by fractures which intersperse the layer at various points (40 m to 90 m and 110 m to 160 m). The fractures are characterised by hyperbolas which are marked in green. The anomaly marked in blue is interpreted to be an air reflection since the slope of the hyperbola is 0.3m/ns. It agrees with observations in the field where the wall of a resort under construction was on the profile path. The diffraction marked in yellow at an elevation of 70 m and at a distance of 150 m along the profile is interpreted to be an example of a duplex or lens shaped body at the subsurface which is created due to the multiple fractures.

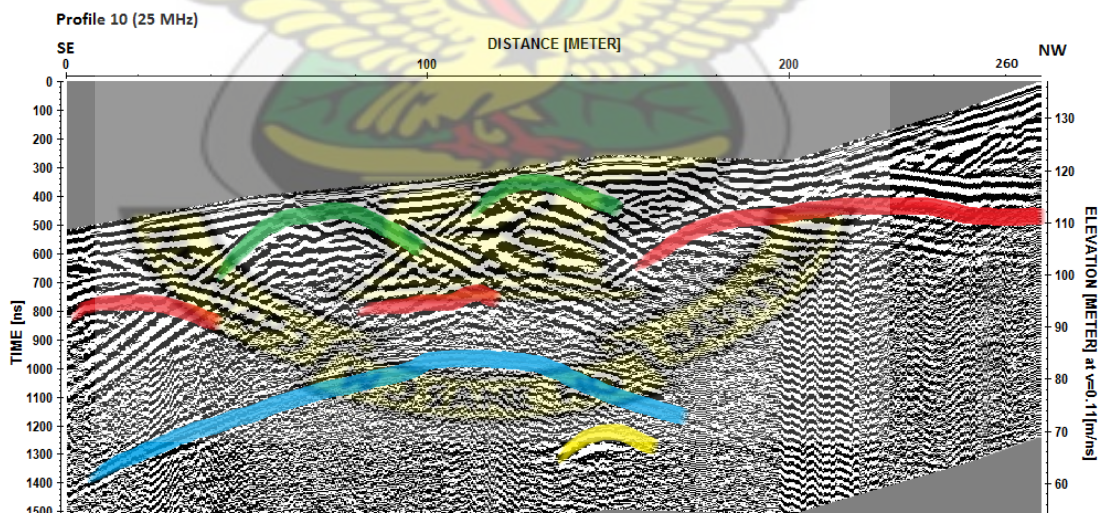


Fig. 4.16: Profile 10 showing marked anomalies.

4.2.11 Profile 11

Figure 4.17 is the 25 MHz section of Profile 11 showing marked anomalies. Profile 11 is 320 m long and has a varied elevation of 106 m at the shore of the lake to 134

m at the end of the profile. The profile extends from the shore in the north-western direction. Three anomalies are prominent on the section of Profile 11. The upper 25 m of the section is characterised by multiple diffractions (some are marked in green in figure 4.17) which are associated with the unconsolidated breccias on the surface of the profile. The breccias cause scattering of the radar signal thereby creating the diffractions on the section. A weak amplitude reflection can be observed from the distance of 80 m to 200 m on the profile and lying between elevations of 100 m and 110 m. This is marked in red and is interpreted to be part of the bedrock.

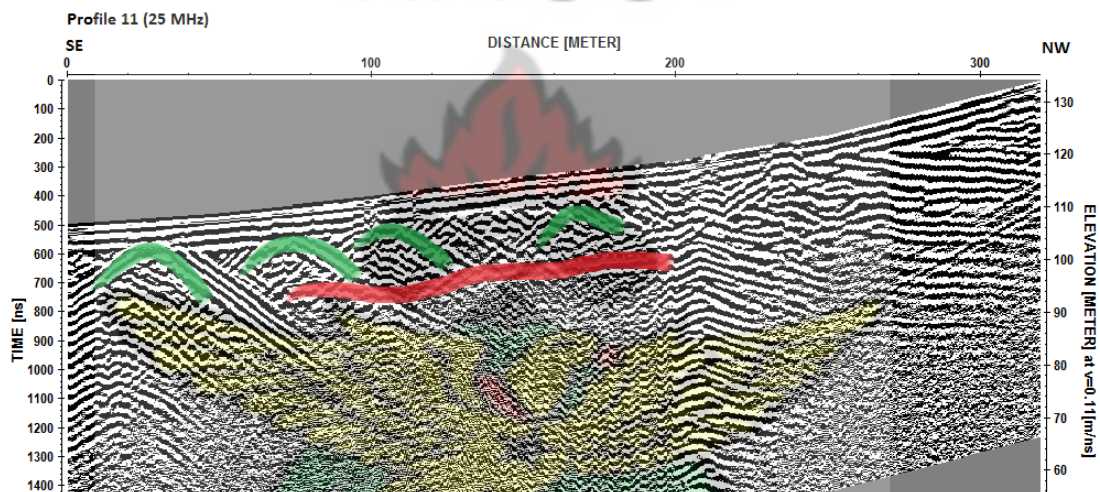


Fig. 4.17: Profile 11 obtained showing marked anomalies.

4.2.12 Profile 12

Figure 4.18 shows the labelled image of Profile 12 using the 25 MHz RTA. Profile 12 is 200 m long and generally extends from the shore in the north-western direction. Elevations along the profile vary from 111 m at the beginning to 126 m at the end of the profile. Signals were attenuated from 90 m downwards. The most significant anomaly present on the section is the unconsolidated layer boundary marked in red.

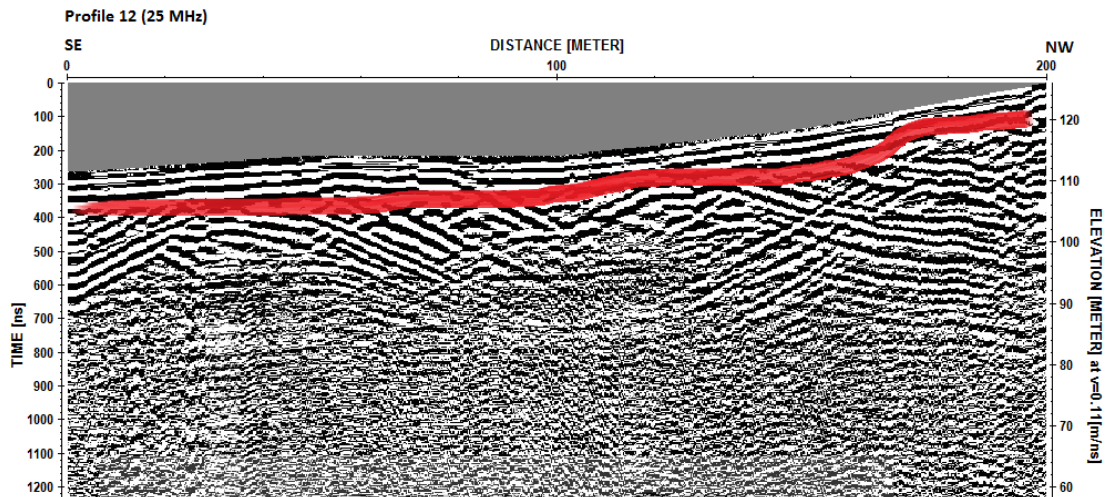


Fig. 4.18: Profile 12 showing marked anomaly.

4.2.13 Profile 15

The marked 25 MHz section of Profile 15 with labelled anomalies is shown in figure 4.19. The profile is 380 m long with an average elevation of 106 m. The profile is aligned in the north-east direction. There are several significant anomalies on the profile. The strong amplitude reflection marked in blue is the unconsolidated breccia layer boundary at a depth of 6 m. A very strong amplitude reflection layer is seen running across the section at an elevation of 110 m (labelled in red). This reflection suggests a water table due to the strong reflection coefficient existing between layers holding groundwater and layers without water. A weak reflection layer interspersed with discontinuities is labelled in green and is suggestive of the perturbed bedrock. Discontinuities are present at a distance of 150 m and 220 m along the profile. The anomaly marked in yellow indicates the presence of an air reflection with a velocity of 0.3 m/ns. This is confirmed by the observation of a hill (an obstruction on the profile path).

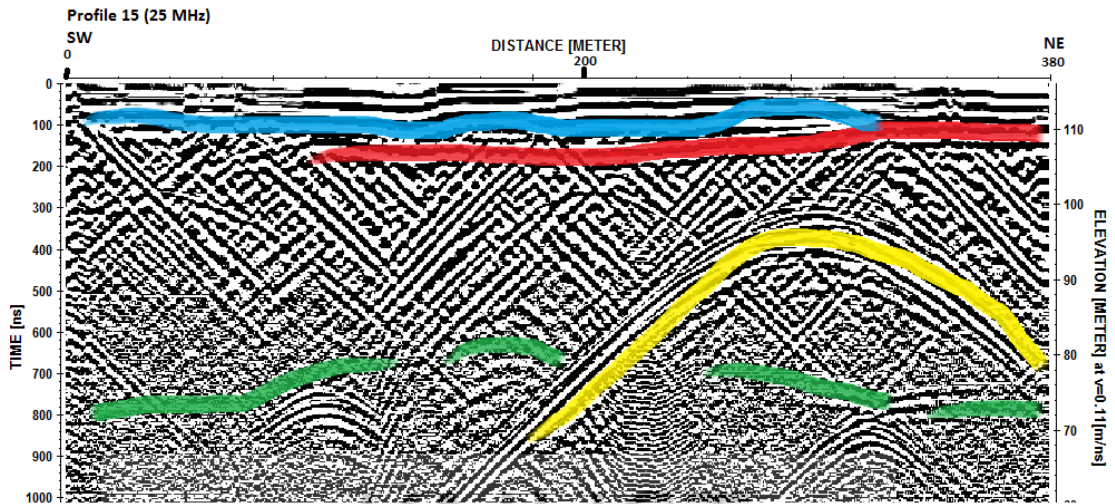


Fig. 4.19: Profile 15 showing marked anomalies.

4.2.14 Profile 16

Profile 16 is 840 m long and is at an elevation of 117 m. The profile is aligned in the southwest-northeast direction. The weak amplitude reflection marked in blue on figure 4.20 is the unconsolidated breccia boundary. This is at a depth of 7 m. The most prominent anomaly on the section is the strong amplitude reflection that runs along the whole profile at an elevation between 106 m and 108 m. This layer is marked in red on figure 4.18 and is suggestive of the water table reflection. Another significant anomaly is a weak reflection layer which breaks at various points.

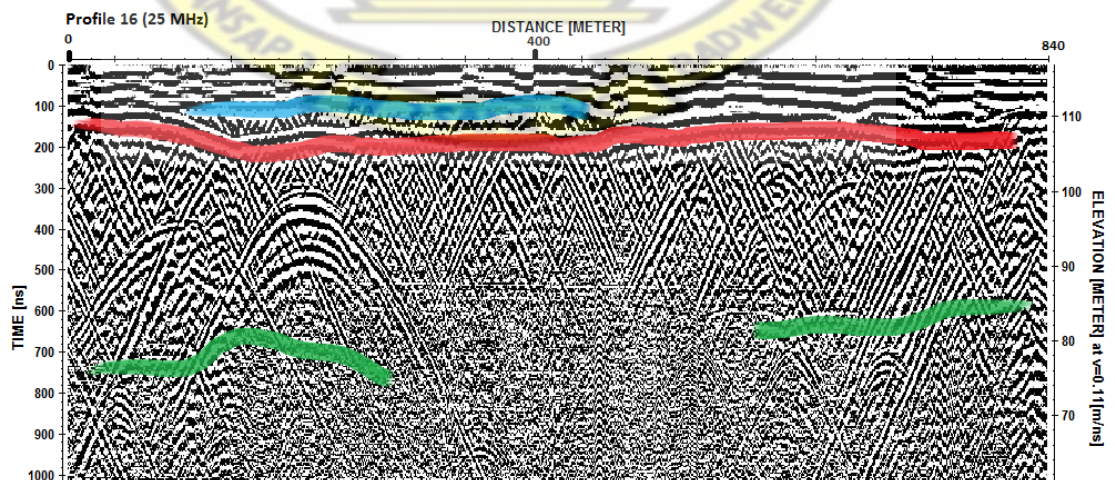


Fig. 4.20: Profile 16 showing marked anomalies.

This layer is marked in green on figure 4.18. It is suggestive of the bedrock layer. From a distance of 250 m to 600 m on the profile exists a fracture characterised by a discontinuity in the layer and an attenuated section.

4.2.15 Profile 17

Profile 17 is 700 m long with an average elevation of 118 m. The profile is aligned in west-east direction. Profile 17's section is characterised by two clearly defined anomalies. A strong reflection at elevation of 100 m is marked in red on figure 4.21 and is indicative of the water table reflection. Characteristic of an impact crater the bedrock is seen as a weak reflection layer labelled in green between elevations of 60 m and 80 m and has breakages at various points along the profile. The breakages are suggestive of fractures due to the hyperbolas characterising them and the attenuated sections. They occur between the distances of 60 m to 160 m, 320 m to 400 m, and 540 m to 640 m.

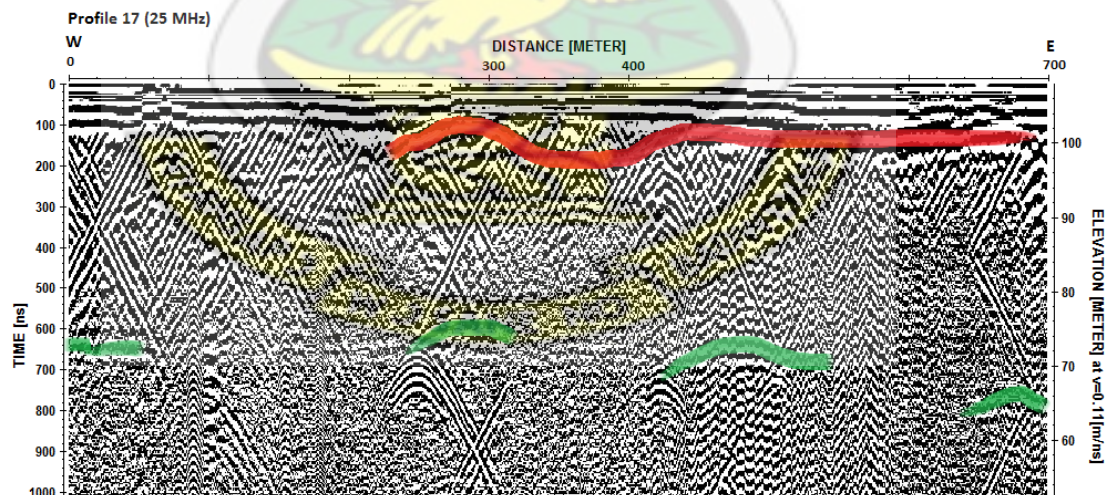


Fig. 4.21: Profile 17 showing marked anomalies.

4.2.16 Profile 18

Figure 4.22 shows the marked anomalies on the section. Profile 18 is 580 m long and is at an elevation of 114 m. The profile is aligned in the southwest-northeast direction. A water table reflection (marked in red on figure 4.22) is present along the whole section varying between the elevations of 96 m and 100 m. A weak reflection layer is observed between the elevations of 50 m and 65 m and is marked in green. This layer represents the bedrock disturbed from the effect of the impact. The bedrock layer is characterised by fractures defined by breakages in the layer and attenuated sections. The fractures occur at distances of 160 m to 300 m and 400 m to 580 m.

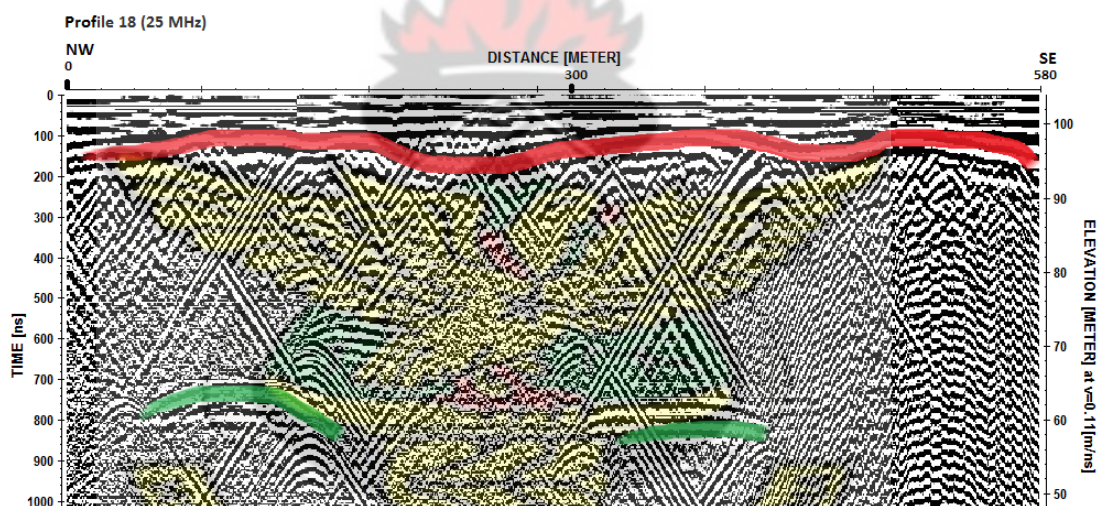


Fig. 4.22: Profile 18 showing marked anomalies.

4.2.17 Profile 19

Profile 19 is 600 m long and at an average elevation of 107 m. The profile is aligned in the north-south direction. Only one significant anomaly was observed on the section. A strong amplitude reflection is observed running along the profile with an elevation varying between 96 m and 100 m. This is suggestive of the water table and is marked in red on figure 4.23. Rapid attenuation is observed after the water

table layer.

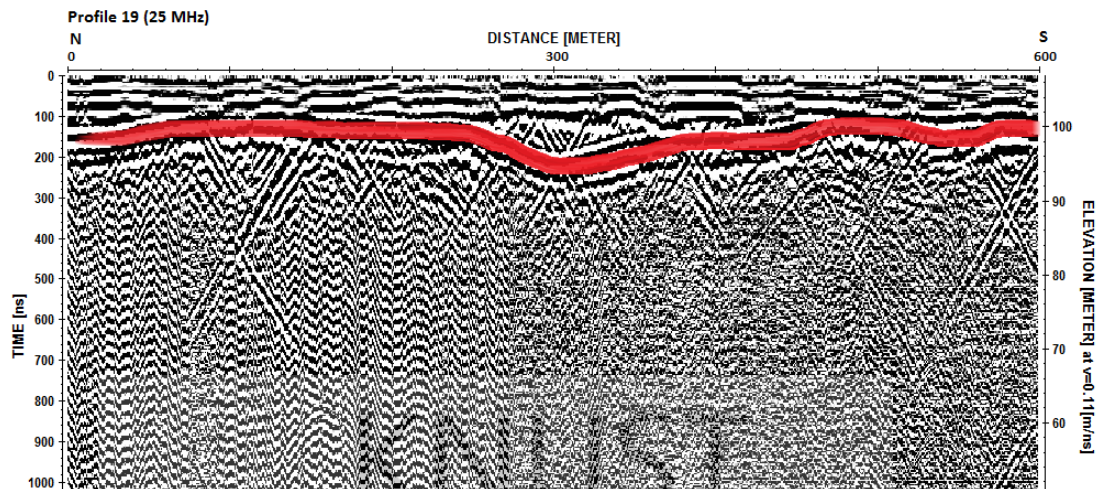


Fig. 4.23: Profile 19 showing marked anomalies.

4.2.18 Profile 20

Profile 20 is 650 m long and at an average elevation of 113 m. The profile is aligned in the northwest-southeast direction. Only one significant anomaly was observed on the section and this is marked on figure 4.24. This is a high amplitude reflection marked in red which indicates the presence of the water table at an elevation of 104 m to 108 m. Radar signals rapidly attenuated after the water table reflection.

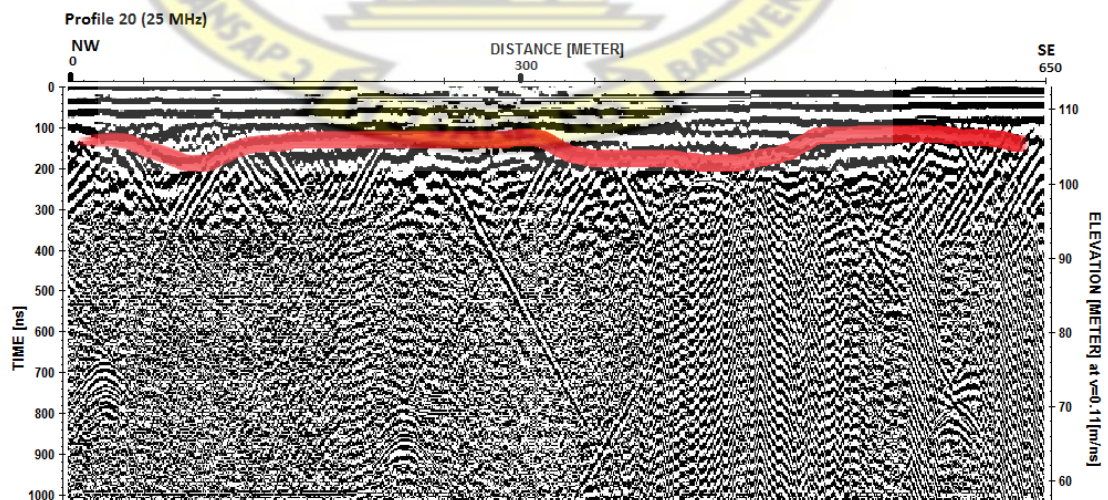


Fig. 4.24: Profile 20 showing marked anomalies.

4.2.19 Profile 21

Profile 21 is 600 m long and is at an average elevation of 117 m. It is aligned in northwest-southeast direction. Significant anomalies are labelled in figure 4.25. The first of these anomalies is a water table reflection which runs along the profile at a varied elevation of between 105 m and 110 m. It is marked in red on figure 4.25. Two reflection layers which are very identical were observed at elevations of 100 m and 80 m respectively (both marked green in figure 4.25). It is suggested that these are mirror images and the actual layer will be at an elevation of 80 m where sections of the perturbed bedrock have been observed on other sections. Mirror images are multiple reflections on the radargram.

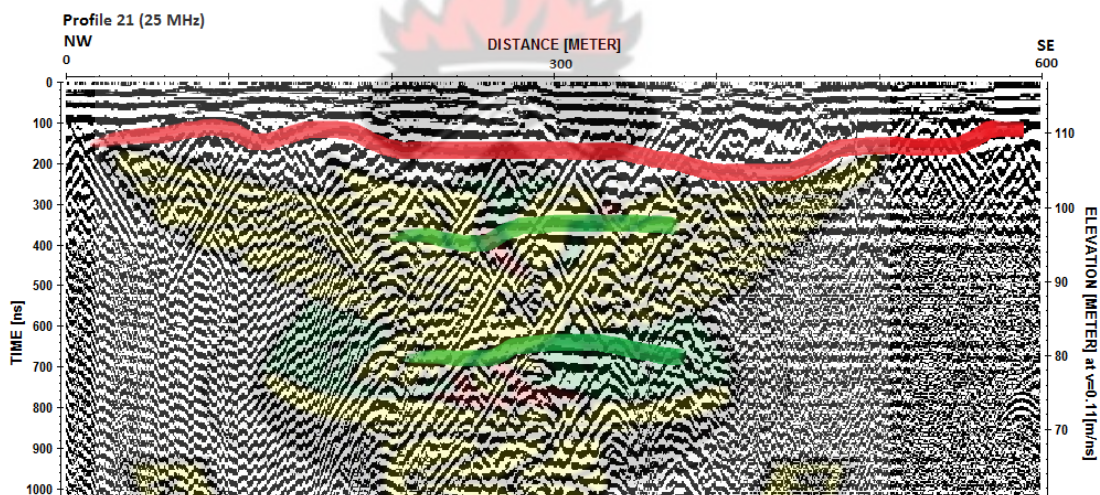


Fig. 4.25: Profile 21 showing marked anomalies.

4.2.20 Profile 22

Profile 22 is 500 m long and is at an average elevation of 112 m. The profile is aligned in the west-east direction. Significant anomalies are shown in figure 4.26. A strong water table reflection with high amplitude is marked in red. The water table lies between the elevations of 104 m to 108 m. At an elevation of about 70 m is a bedrock layer which has breakages. These breakages are interpreted to be fractures

due to the hyperbola and attenuated sections characterising their locations. They are located between the distances of 100 m to 280 m and from 380 m to 460 m.

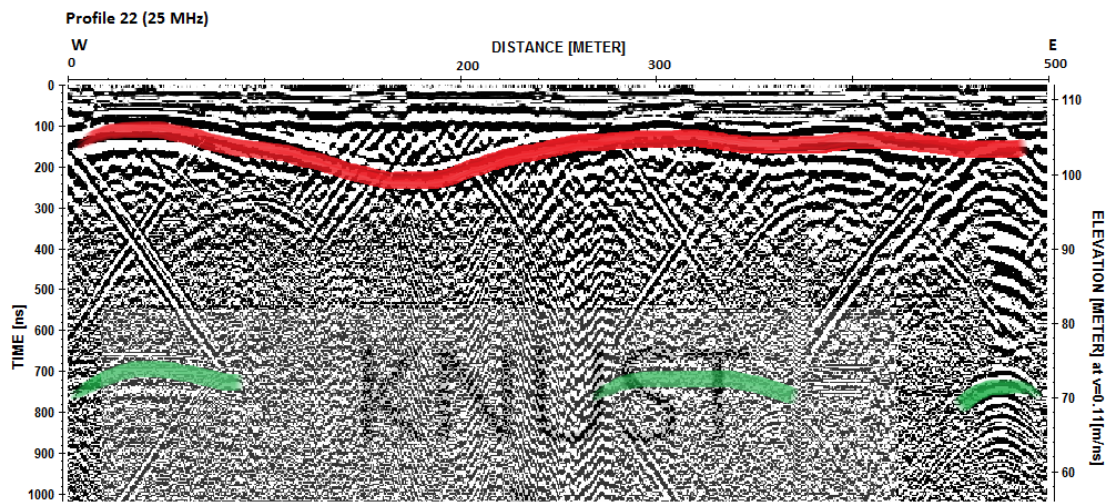


Fig. 4.26: Profile 22 showing marked anomalies.

4.3 Interpretations of Radargrams

It is observed that the resolution of the sections of Profile 15 to Profile 22 is better than the sections of profile 1 to profile 12. In Profile 1 to profile 12 subsurface structures resolved are few and attenuation is rapid across the profiles. In Profile 15 to profile 22 however coherent stratigraphic horizons are resolved clearly. All the sections were observed to include diffractions on the upper 25 m of the surface but Profile 1 to 12 showed much more clutter on the sections. The presence of diffraction hyperbolas on a GPR section is indicative of fractures, folds, and dikes. Perturbed bedrocks and unconsolidated breccia can also cause diffraction hyperbolas.

The reason advanced for the presence of numerous diffractions on the radargrams of profile 1 to profile 12 is the presence of breccias from weathering in the tropical climate of the study area. Weathering due to erosion by running water and temperature changes have caused the accumulation of unconsolidated material on the surface of the slopes (Profiles 1 to 12). Since breccias along these profiles are unconsolidated, radar signal is scattered and attenuated so resolution is no deeper

than a few metres in some cases. Profiles 15 to profile 22 however show clear coherent horizons with discontinuities associated with fractures.

Comparing the 25 MHz sections and 50 MHz sections in figure 4.5 and 4.6 confirmed that the 25 MHz central frequency resolved deeper subsurface features than the 50 MHz central frequency. The shallow subsurface features were however more clearly resolved by the 50 MHz central frequency.

Of the three migration algorithms applied, it is observed from comparisons in figure 4.1 to 4.4 that the diffraction stack gave the best results. Sections migrated with the diffraction stack algorithm successfully migrated subsurface features to their true depths and collapsed hyperbolas on the sections.

4.4 Stratigraphic Horizons

The subsurface of the impact crater is characterised by strata with clear horizons on the sections and discontinuities across the stratas. The first of these layers is associated with unconsolidated material within the crater. The Bosumtwe crater is located in a tropical region of the world, and the inner morphological crater has steep slopes. Therefore weathering occurs on a large basis. This causes the accumulation of breccias along the slopes of the inner morphological crater. Secondly, rapid siltation in the lake region is occurring due to the presence of the unconsolidated breccias. Confirming this is the presence of a strong reflection layer present on sections of Profile 3 (figure 4.9), Profile 4 (figure 4.10), Profile 5 (figure 4.11), Profile 7 (figure 4.13), and Profile 9 (figure 4.15), Profile 12 (figure 4.17), Profile 15 (figure 4.19) and Profile 16 (figure 4.20). The breccia layer has a minimum depth of 4 m and a maximum of 7 m in the Bosumtwe crater.

4.4.1 Bedrock Layer

Observations made on sections of Profile 2 (figure 4.8), Profile 3 (figure 4.9), Profile 6 (figure 4.12), Profile 8 (figure 4.14), Profile 9 (figure 4.15), Profile 10 (figure 4.16), Profile 11 (figure 4.17), Profile 15 (figure 4.19), Profile 16 (figure 4.20), Profile 17 (figure 4.21), Profile 18 (figure 4.22), Profile 21 (figure 4.25) and Profile 22 (figure 4.26) indicate the presence of a significant anomaly with a varied depth between 10 m to 44 m. The layer is interspersed with discontinuities and amplitudes of reflected signals are weak. The layers observed in the above figures are associated with a bedrock layer which was shattered during the impact event.

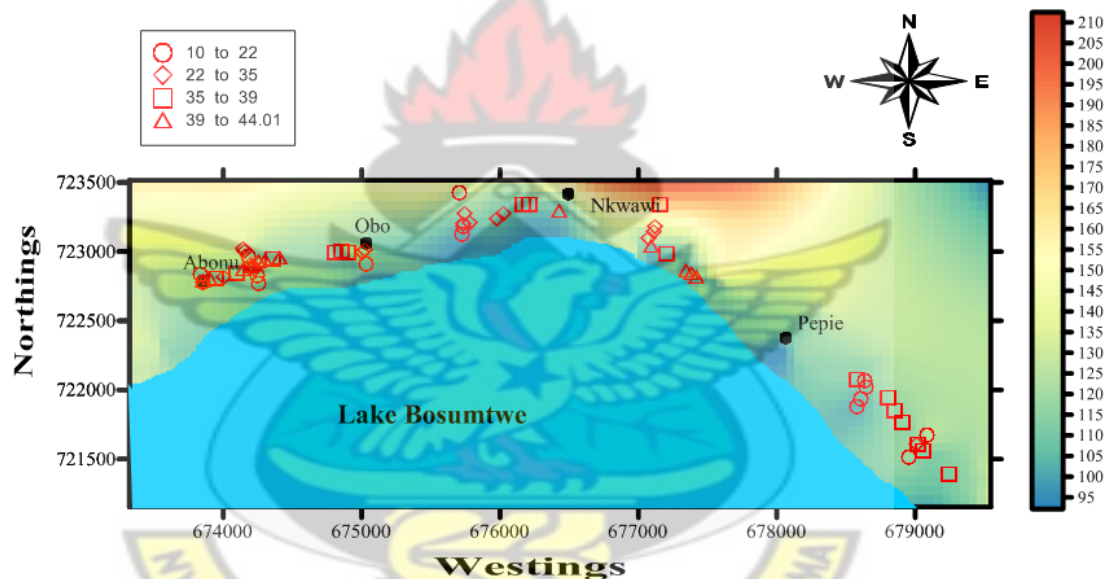


Fig. 4.27: Depth to bedrock variation within Northern section of Bosumtwe Crater.

Figure 4.27 is a visual representation of the depth to bedrock at various locations within the northern section of Bosumtwe crater. Generally depth to bedrock in the region varies from about 10 m to 44 m. From the classed post map in figure 4.25, it is observed that the deepest bedrock occurs at the western side of the map (near the town of Abonu). The shallowest bedrock occurs in the eastern side of the crater.

4.5 Depth to Water table

To define the depth to water table, sections of profiles 15 to 22 were assessed and compared to the levels of water in the lake. The water table is the high amplitude reflection observed running along the sections in figures 4.11, 4.19, 4.20, 4.21, 4.22, 4.23, 4.24, 4.25 and 4.26. Figure 4.28 is a class post map of the variation of the water table elevation.

The water table varied between depths of 5 m to 12 m within the crater. This depth is consistent over the whole section of the study area. The shallowest section of the water table occurs in the southeastern section of the study area. The deepest section of the water table occurs in the northern section of the study area. This agrees with physical observation in the field since the northern section has a lot of sandy overburden.

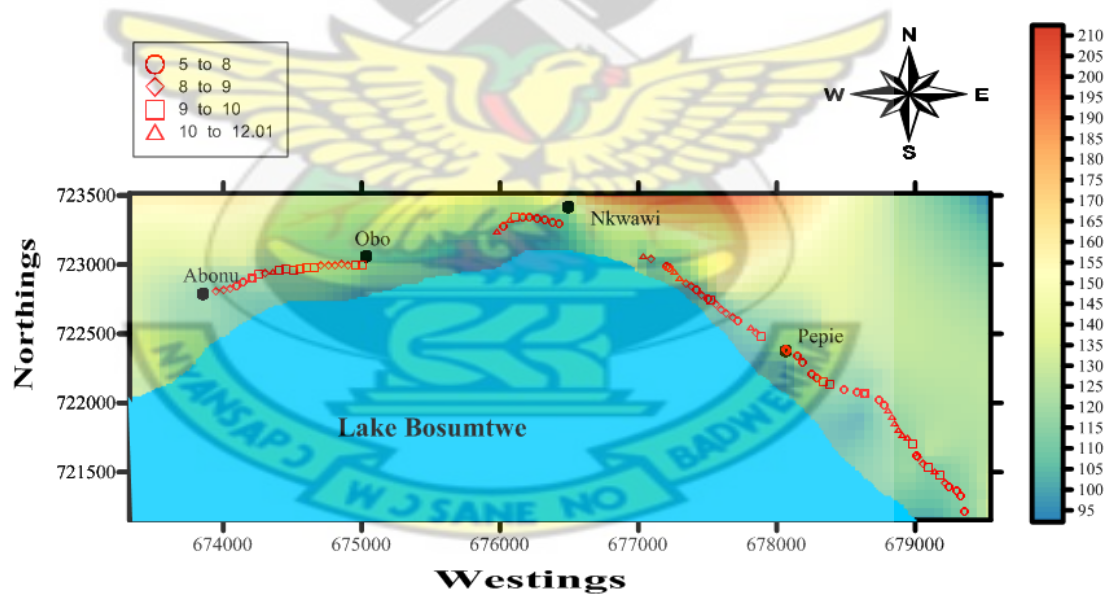


Fig. 4.28: A classed post map show water table variation within the Northern section of the Bosumtwe impact crater.

Table 4.1 compares the elevation of the water table and the elevation of the lake level near the shore at various positions. The water table within the crater is at a

similar elevation as the elevation of the lake at the shore. This implies there is interaction between water in the lake and the groundwater on the shore (within the crater). It is suggested that the water in the lake fills the pores of the rocks within the crater. Koeberl and Reimold have stated in their paper of 2005 that the lake had previously higher levels and had occupied the whole crater and even overflowing at a point in time.

If this is the case, it will imply that the inner morphological crater may have been a lake bed at a point in time. It can be observed that the water table is quite near the surface in some locations.

Table 4.1: Water table elevation and lake level elevation

Profile Name	Water table Elevation (within crater)	Maximum Lake Elevation Level at Shore	Minimum Lake Elevation Level at Shore
15	108	108	106
16	108	110	105
17	100	104	98
18	99	99	95
19	99	100	94
20	105	106	102
21	110	110	104
22	99	106	98

In the light of the high water table and the porosity of the rocks within the crater, interaction between surface pollutants and groundwater is a great possibility. This is even more likely due to the heavy use of chemicals in the farming of cocoa (the most widespread crop grown in the area) a major cash crop in Ghana. It is suggested that there is interaction between the surface water and groundwater through the numerous fractures identified within the crater.

4.6 Fracture Distribution

The area in which this study was conducted in falls within a zone which is characterised by dominant thrust faulting of multiple orientations according to the work done by (Reimold, et al. 1998). Sections of the profiles taken across the study area also proved this observation.

Fractures and folds on GPR sections are marked by diffractions and attenuated signals. Fractures were observed on the sections of Profile 1 (figure 4.7), Profile 7 (figure 4.13), Profile 9 (figure 4.15), Profile 10 (figure 4.16), Profile 16 (figure 4.20), Profile 17 (figure 4.21), Profile 18 (figure 4.22), and Profile 22 (figure 4.26).

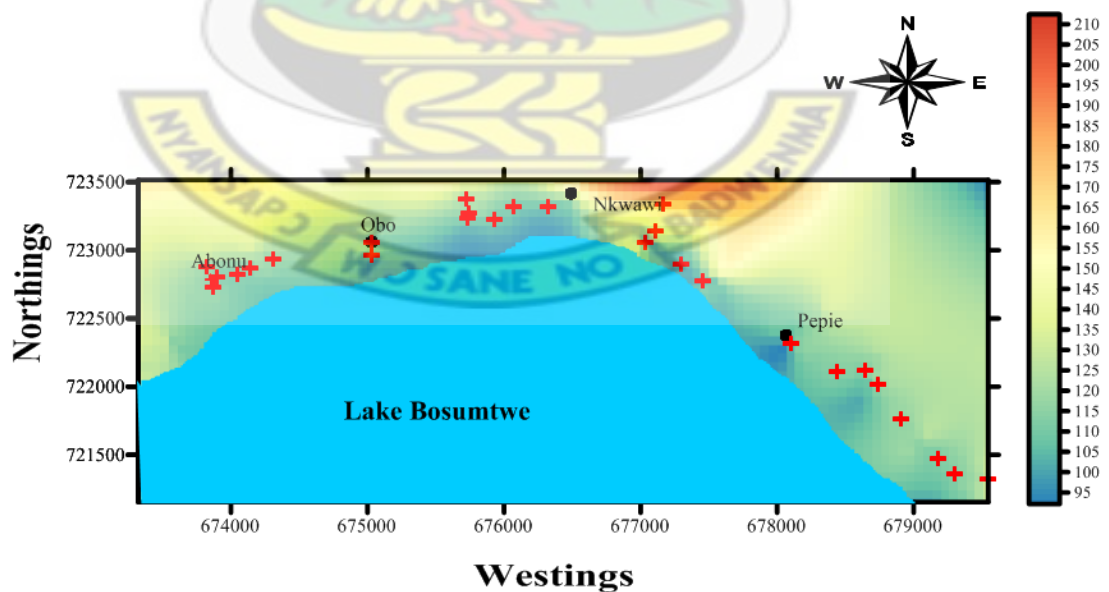


Fig. 4.29: A post map showing fracture distribution within the northern sector of Bosumtwé crater.

Fractures observed on the 25 MHz sections are mapped in the post layer on the image map of the northern sector of the Bosumtwe crater (figure 4.29). The most important observation on the map is the presence of multiple fractures near Abonu and Obo, the two towns with the highest concentration of resorts in the Bosumtwe crater.

KNUST



CHAPTER FIVE

CONCLUSION AND RECOMMENDATIONS

5.0 Conclusion and Recommendations

5.1 Conclusion

Within the study area, radar signals penetrated to as much as 60 m into the ground. On the profiles taken perpendicular to the shore however (1 to 12) signals were attenuated by the existence of unconsolidated breccias and fractures of multiple orientations just below the surface. High resolution images of the subsurface were acquired on profiles taken parallel to the shore (15 to 22). Strong, coherent stratigraphic horizons were identified on these profiles.

The 25 MHz prospecting frequency resolved features at deeper depths than the 50 MHz prospecting frequency while the 50 MHz prospecting frequency resolved shallow features better than the 25 MHz prospecting frequency. This is an already well known fact in relation to GPR surveys; that lower frequencies resolve deeper subsurface features. This fact is reinforced by the research.

The GPR method was able to clearly resolve subsurface features such as the subsurface layers, fractures and the water table. The subsurface of the Bosumtwe crater is characterised by two layers. The first layer is made up of unconsolidated breccia that has accumulated due to the impact event and weathering over time. The second layer is the bedrock layer. This layer is perturbed and shattered agreeing with literature on crater subsurfaces. The depth to bedrock varies from 10 m to 44 m within the crater.

The depth to water table varies from 5 m to 12 m within the Bosumtwe crater. Groundwater within the crater interacts with the water in the lake. Contaminants from farming activities and other human activities, seeping into the lake is a distinct

possibility. With the wide distribution of fractures within the crater area the high lake level will push up the water table onshore and this will lead to pollutants seeping through the fractures back into the lake.

The presence of numerous fractures within the inner morphological crater poses a hazard to human settlements within the crater area. Due to the fractures within the subsurface, blocks of rocks on the the slopes are easily washed away during the rainy season. This is a potential landslide hazard. Buildings within the crater area will be threatened by this development. Lake Bosumtwe is also in danger due to rapid siltation.

Images from the GPR data suggest that the diffraction stack time migration can best be used in effectively removing diffractions and migrating horizons to their actual depths. The results are high resolution images.

5.2 Recommendations

To confirm the contamination theory, it is recommended that a physico-chemical analysis of water samples from Lake Bosumtwe be undertaken. GPR can also be used to trace contaminant paths through the subsurface.

Different geophysical methods for delineating stratigraphy, fractures and depth to water table should be applied in the study area for an integrated interpretation to be done. It is recommended that the seismic reflection method is applied. It is also recommended that geophysical methods that can clearly define fracture orientation should be applied in the study area such as azimuthal surveys and other electromagnetic surveys.

Results from this survey have conclusively suggested the risk of easy contamination of the lake and groundwater. It is suggested that the Bosumtwe District Assembly promulgate bye laws for the commissioning of an environmental impact assessment

regime for the crater area. Resorts and hotels to be built in the area should also conduct impact assessment surveys before they are allowed to be built due to the existence of fractures in the study area. A disaster management regime should be set up for the crater zone.

KNUST



References

- Annan A. P. (2002). GPR-History, trends and future developments. *Subsurface Sensing Technologies and Applications* 3, no. 4.
- Annan A. P., and Davis, J. L. (1977). *Radar range analysis for geological materials*. PEMD #10, Mississauga, Ontario: Sensors and Software Inc.
- Annan A. P., and Davis, J. L. (1988). Radar sounding in potash mines: Saskatchewan, Canada. *Geophysics* 53: 1556-1564.
- Bevan B. W. (1991). The search for graves. *Geophysics* 56, no. 9: 1310-1319.
- Bevan B. W., and Kenyon J. (1975). Ground Penetrating Radar for historic archeology. *MASCA Newsletter* 11, no. 2: 2-7.
- Boamah Daniel, and Koeberl Christian (2003). Geology and geochemistry of shallow drill cores from the Bosumtwi impact structure. *Meteoritics and planetary science*: 1137-1159.
- Bosumtwi District Assembly (2006). *Bosumtwi Tourism Attractions*. http://bosomtwe.ghanadistricts.gov.gh/?arrow=atd&_=20&sa=983 (accessed April 12, 2012).
- . *Physical Characteristics*. http://bosomtwe.ghanadistricts.gov.gh/?arrow=atd&_=20&sa=4555 (accessed April 12, 2012).
- Boyce J. M., and Mouginiis-Mark P. J. (2006). Martian craters viewed by the THEMIS instrument: Double-layered ejecta craters. *J. Geophys. Res* 111.
- Chapman C. R., and Morrison D. (1994). Impacts on the earth by asteroids and comets: Assessing the hazard. *Nature* 367: 33-40.
- Coon J. B., Fowler J. C., and Schafers C. J. (1981). Experimental uses of short pulse radar in coal seams. *Geophysics* 46: 1163-1168.
- Curtiss D. K., and Wavrek D. A. (1998). Hydrocarbons in meteorite impact structures: Oil reserves in the Ames feature. *Journal of the Minerals (Metals and Materials Society)* 50: 35-37.
- Daniels D. J., Gunton, D. J. and Scott, H. F. (1988). Introduction to subsurface radar. *IEE Proceedings* 135: 278-320.
- Danour Sylvester K. (20 February 2012), Personal Communication.
- Davis J. L., and Annan A. P. (1989). Ground-penetrating radar for high resolution mapping of soil and rock stratigraphy. *Geophysical Prospecting* 37, no. 5: 531-559.
- Dobrin M. H. (1976). *Introduction to Geophysical prospecting*. New York: McGraw-Hill.

- Doolittle J. A. (1993). Characteristics and monitoring the vadose zone with ground penetrating radar. *Advanced Ground Penetrating Radar: Technologies and Applications* (Ohio State University): 105-119.
- Dressler B. O., Morrison, G. G., Peredery, W. V and Rao B. V. (1987). The Sudbury structure, Ontario, Canada - A review. In *Research in Terrestrial Impact Structures*, by J. Pohl, 39-68. Braunschweig/Weisbaden: Friedr. Vieweg and Sohn.
- Fisher E., McMechan G. A., Annan A. P., and Cosway S. W. (1992). Acquisition and processing of wide aperture ground penetrating radar data. *Geophysics* 57, no. 4: 495.
- Garvin J. B, Campbell B. A., Zisk S. H., Schaber G. G., and Evans C. (1989). Radar scattering mechanisms within the meteor crater ejecta blanket: Geologic implications and relevance to Venus. *Abstracts for the Venus Geoscience Tutorial and Venus Geologic Mapping Workshop*: 19-20.
- Gault D. E. (1968). Impact cratering mechanics and structures. In *Shock Metamorphism of Natural Materials*, by B. M. French and N. M. Short, 87-100. Baltimore: Mono Book Corp.
- Grant J. A., Schultz P. H., and Campos-Enriquez J. O. (1995). Definition of shallow subsurface structure around the Chicxulub impact crater using Ground Penetrating Radar. *Abstracts of the Lunar and Planetary Science Conference* 26: page 495.
- Grasmueck Mark (1996). 3-D ground penetrating radar applied to fracture imaging in gneiss. *Geophysics*: 1050-1064.
- Greeley R., Christensen P. R., and McHone J. (1987). Radar characteristics of small craters-Implications for Venus. *Earth Moon Planets* 37: 89-111.
- Grasmueck Mark, Weger Ralf, and Horstmeyer Heinrich (2005). Full resolution 3D GPR imaging. *Geophysics* 70, no. 1.
- Heggy Essam, and Paillou Philippe (2006). Probing structural elements of small buried craters using ground-penetrating radar in the southwestern Egyptian desert: implications for Mars shallow sounding. *Geophysical Research Letters* 33.
- Huggenberger P., Meier P., and Pugin A. (1994). Ground probing radar as a tool for heterogeneity estimation in gravel deposits: advances in data processing and facies analysis. *Journal of Applied Geophysics* 31, no. 1-4: 171-184.
- Jones W. B. (1985a). Chemical analyses of Bosumtwi crater target rocks compared with Ivory Coast tektites. *Geochimica et Cosmochimica Acta* 49: 2569-2576.
- Jones W. B., Bacon M., and Hastings D. A. (1981). The Lake Bosumtwi impact crater, Ghana. *Geological Society of America Bulletin* 92: 342-349.
- Junner N. R. (1937). The geology of the Bosumtwi caldera and surrounding country. *Gold Coast Geological Survey Bulletin* 8: 1-38.

- Kenkmann, T., Artemieva N. A., Wunnemann K., Poelchau M. H., Elbeshausen D., and Nunez del Prado H. (2009). The Carancas meteorite impact crater, Peru: geologic surveying and modeling of crater formation and atmospheric passage. *Meteoritics and Planetary Science*: 985-1000.
- Koeberl C. (1994a). African meteorite impact craters: Characteristics and geological importance. *Journal of African Earth Sciences* 18: 263-295.
- Koeberl C., and MacLeod K. (2002). Catastrophic events and mass extinctions: impacts and beyond. *Geological Society of America Special Paper* 356: 746.
- Koeberl C., Bottomley R. J., Glass B. P., and Storzer D. (1997a). Geochemistry and age of Ivory Coast tektites and microtektites. *Geochimica et Cosmochimica Acta* 61: 1745-1772.
- Koeberl C., Reimold W. U., Blum J. D., and Chamberlain C. P. (1998). Petrology and geochemistry of target rocks from the Bosumtwi impact structure, Ghana and comparison with Ivory Coast tektites. *Geochimica et Cosmochimica Acta* 62: 2179-2196.
- Koeberl Christian, and Reimold Wolf U. (2005). Bosumtwi impact crater Ghana (West Africa): An updated and revised geological map, with explanations. *Jahrbuch Der Geologischen Bundesanstalt*: 31-70.
- Maijala P. (1992). Application of some seismic data processing methods to ground penetrating radar. *Fourth International Conference on Ground Penetrating Radar*. Rovaniemi: Geological Society of Finland. 365 pages.
- Mala Geoscience (accessed April 21, 2012). *Mala Products*. 2012. <http://www.malags.com/Products>.
- McClymont Alastair, Streich Rita, Heincke Björn, and Green Alan (2006). Visualization of active faulting using 3-D GPR data recorded across the Alpine Fault, New Zealand. *11th International Conference on Ground Penetrating Radar*. Columbus Ohio.
- Melosh H. J.(1989). *Impact Cratering: A Geologic Process*. Oxford: Oxford University Press.
- Milsom John (2003). *Field Geophysics*. Wiley.
- Moon P. A., and Mason D. (1967). The geology of 1/4 field sheets nos. 129 and 131, Bompata S.W. and N.W. *Ghana Geological Survey Bulletin* 31: 1-51.
- Neukem G., Ivanov B. A., and Hartmann W. K. (2001). Cratering records in the inner solar system in relation to the lunar reference system. In *Chronology and Evolution of Mars*, by R. Kallenbach, J. Geiss and W. K. Hartmann, 87-104. Bern: International Space Science Institute.
- Nickel H., Sender F., Thierbach R., and Weichart A. (1983). Exploring the interior of salt domes from boreholes. *Geophysical Prospecting* 31, no. 1: 131-148.

Olhoeft G. R. (1987). Electrical properties from 10^{-3} to 10^{+9} Hz—physics and chemistry. *2nd International Symposium on the Physics and Chemistry of Porous Media*. American Institute of Physics. 281–298.

Olhoeft G. R. (1975). *The electrical properties of permafrost*. PhD Thesis, Toronto: University of Toronto.

Planetary and Space Science Centre (accessed April 20, 2012). *Earth Impact Database*. 2012. <http://www.passc.net/EarthImpactDatabase/index.html>.

Poelchau Michael H. (2010). *The subsurface structure of oblique impact craters*. PhD Thesis, Berlin: vom Fachbereich Geowissenschaften der Freien Universität Berlin.

Rees H. V., and Glover J. M. (1992). Digital enhancement of ground probing radar data. Edited by J. Pilon. *Ground Penetrating Radar* (Geological Survey of Canada) 90, no. 4: 187-192.

Reimold Wolf U., Brandt Dion, and Koeberl Christian (1998). Detailed structural analysis of the rim of a large complex impact crater: Bosumtwi, Ghana. *Geology*: 543-546.

Reynolds John M. (1997). *An introduction to applied and environmental geophysics*. John Wiley and Sons.

Roulston M. S., and Ahrens T. (1997). Impact and frequency of SL9-Type events on Jupiter. *Icarus*, no. doi:10.1006/icar.1996.5636, 138–147.

SEG. *SEG Digital Library*. 2012. <http://scitation.aip.org/servlet/SearchSegDict?&sourceQuery=id&ResultMaxDocs=500&sort=reldocsPerPage=50&queryText=NE000033&DISPLAY=YES> (accessed March 6, 2012).

Sensors and Software Inc. (1999). *Practical processing of GPR data*. Proceedings of the Second Government Workshop on Ground Penetrating Radar, Mississauga: Sensor and Software.

Shoemaker E. M. (1976). Why study impact craters. *Proceedings of the Symposium on Planetary Cratering Mechanics*. New York: Pergamon Press Inc. 1-10.

Steeple Don W. (2001). Engineering and environmental geophysics at the millenium. *Geophysics*: 31-35.

Stoffler D., and Langenhorst F. (1994). Shock metamorphism of quartz in nature and experiment: I. Basic observation and theory. *Meteoritics* 29: 155-181.

Stöffler D., and Ryder G. (2001). Stratigraphy and isotope ages of lunar geological units: chronological standards for the inner solar system. *Space Science Review*: 9–54.

Thierbach R. (1974). Electromagnetic reflections in salt deposits. *Journal of Geophysics* 40: 633-637.

United Nations. *Millenium Development Goal 7*. (2010).

<http://www.un.org/millenniumgoals/envIRON.shtml> (accessed April 28, 2012).

Woodfield P. D. (1966). The geology of the 1/4 field sheet 91, Fumso, N.W. Ghana. *Ghana Geological Survey Bulletin* 30: 1-66.

KNUST



APPENDIX: GPS Locations of Initial Point of Profiles

Profile Name	GPS Location UTM	Elevations
1	30 0679219 0721153	105
2	30 0678953 0721518	118
3	30 0678582 0721878	101
4	30 0678008 0722291	93
5	30 0677502 0722728	109
6	30 0676999 0723026	100
7	30 0676403 0723241	100
8	30 0675726 0723129	101
9	30 0675040 0722862	98
10	30 0674260 0722775	108
11	30 0673887 0722673	106
12	30 0673655 0722273	111
15	30 0673850 0722792	113
16	30 0674210 0722904	115
17	30 0675731 0723202	105
18	30 0677035 0723062	101
19	30 0677519 0722745	99
20	30 0678066 0722382	108
21	30 0678640 0722067	111
22	30 0679020 0721604	108